Eidgenössische Technische Hochschule Zürich
Swiss Federal Institute of Technology Zurich

Sensory-Motor Systems Lab

Deutsches Zentrum
für Luft- und Raumfahrt e.V.

Development of a Calibration Routine for Remotely Controlling a Robotic Hand

Master Thesis at the
Sensory-Motor Systems Group
Prof. Dr. Robert Riener
Department of Mechanical & Process Engineering
ETH Zurich

by
Ozan Çaldıran

Thesis advisor:
Prof. Dr. Robert Riener
Thesis Supervisor:
Katharina Hertkorn
Philipp Kremer
Registration date: Mar 07th, 2011
Submission date: Aug 31st, 2011

Contents

Abstract **xiii**

Acknowledgements **xv**

Conventions **xvii**

1 Introduction **1**

1.1 Motivation 1

1.2 The Telepresence System 4

1.3 Slave Side: DLR/HIT Hand II 5

1.4 Master Side: Dataglove 7

1.5 The Goal of the Thesis 8

2 Friction Compensation **13**

2.1 Related Work 14

2.1.1 Possible Friction Models 16

2.1.2 Parameter Identification for a Friction Model 17

2.2 Own Work 21

2.2.1 Parameter Identification Routine . . . 21

2.2.2 A Graphical User Interface for the Identification of the Friction Parameters 24

3 Controller Design 27

3.1 Related Work 28

3.2 Own Work 35

4 Calibration and Mapping of the Cyberglove 39

4.1 Related Work 39

4.1.1 Former Calibration Routine 40

4.1.2 An Improvement of the Former Calibration Routine 42

4.2 Own Work 44

4.2.1 Instability 45

4.2.2 Infeasible Solutions 46

5 Experimental Evaluation 47

5.1 Experimental Setup 47

5.2 Friction Compensation 48

5.3 Comparison of a Disturbance Observer Based Functional Controller with a PD Controller 56

5.4 Calibration and Mapping of the Cyberglove . 61

6 Summary and Future Work 67

6.1 Summary and contributions 67

6.2 Future work 68

A A Matlab GUI for Friction Parameter Identification 71

B Controller Evaluation for Blended Reference 75

Bibliography 81

List of Figures

1.1 The telepresence system 5

1.2 Cyberglove 5

1.3 DLR/HIT Hand II 6

1.4 Cyberglove together with the HMI 6

1.5 Bevel gears at the base joint 7

1.6 Cyberglove sensor locations 8

1.7 Cyberglove kinematics 9

1.8 DLR/HIT Hand II kinematics 10

2.1 Candidate friction models 17

2.2 Comparison of friction parameter estimation routines 23

2.3 Comparison of friction parameter estimation routines 23

2.4 Matlab GUI for parameter identification routine 24

2.5 Flowchart of parameter identification routine 26

3.1 Design framework of bilateral system 28

3.2 Disturbance observer [Tsuji et al., 2006] . . . 29

3.3 Bilateral systems with different couplings . . 30

3.4 Grasping task [Tsuji et al., 2007] 30

3.5 Control of functionally related systems 31

3.6 Virtual plant [Sabanovic and Ohnishi, 2011] . 34

3.7 Control scheme for the DLR/HIT Hand II . . 36

4.1 Predefined hand poses used by the old calibration routine [Huenerfauth and Lu, n.d] . . 41

4.2 Pinch pose [Huenerfauth and Lu, n.d] 42

4.3 Example hand poses used by the new calibration routine 44

5.1 Comparison of estimation errors for the 2^{nd} motor 49

5.2 Comparison of estimation errors for the 3^{rd} motor 49

5.3 Maximum and minimum estimated friction for the 2^{nd} motor 50

5.4 Maximum and minimum estimated friction for the 3^{rd} motor 50

5.5 Difference of maximum and minimum estimated friction for the 2^{nd} motor 51

5.6 ifference of maximum and minimum estimated friction for the 3^{rd} motor 51

5.7 Commanded torque vs estimated torque for the 2^{nd} motor 52

5.8 Commanded torque vs estimated torque for the 3^{rd} motor 52

5.9 Blended trajectory profile 53

5.10 DOB estimation vs friction model estimation for the 2^{nd} motor with external torque 54

5.11 DOB estimation vs friction model estimation for the 3^{rd} motor with external torque 55

5.12 DOB estimation vs friction model estimation for the 2^{nd} motor with step position reference 56

5.13 DOB estimation vs friction model estimation for the 3^{rd} motor with step position reference 57

5.14 DOB estimation vs friction model estimation for the 2^{nd} motor with blended trajectory reference 58

5.15 DOB estimation vs friction model estimation for the 3^{rd} motor with blended trajectory reference 59

5.16 DOB estimation vs friction model estimation for the 2^{nd} motor 60

5.17 DOB estimation vs friction model estimation for the 3^{rd} motor 61

5.18 Movement directions for the comparison . . 62

5.19 Step reference - responses of the DOB based controller and the PD controller 66

A.1 Low motor limit for 1^{st} motor 71

A.2 High motor limit for 1^{st} motor 72

A.3 Low motor limit for 2^{nd} motor 72

A.4 High motor limit for 2^{nd} motor 73

A.5 Low motor limit for 3^{rd} motor 73

A.6 High motor limit for 3^{rd} motor 74

A.7 Wait for start command 74

B.1 Blended trajectory reference- responses of the DOB based controller and the PD controller 79

List of Tables

2.1 Estimation results of Connette [2006] 20

2.2 Estimation results - fixing c [Connette, 2006] 20

2.3 Estimation results - fixed I [Connette, 2006] . 20

2.4 Estimation results for old routine 21

2.5 Estimation results for the new routine 22

Abstract

Maintenance and de-orbiting of satellites are tasks that are yet to be solved. One of DLR's approach to this task is to on-orbit servicing is using a telepresence system. High performance telepresence systems enable intuitive interaction with the remote environment. There are several factors influencing the overall performance like the level of immersion of the video display. This work focuses on improving the coupling between the hands, DLR/HIT Hand II, of the remotely located humanoid robot Justin and the hands of the human operator. In order to ensure improved coupling of the two, both the ability of the DLR/HIT Hand II to track given references, and the calibration and mapping of a dataglove, which measures the human hand joint angles, are improved. This is achieved by three main tasks: implementing a friction compensation module with a friction parameter identification routine, designing a controller based on the functionally related systems framework, and developing a calibration routine that handles the calibration and mapping of a dataglove simultaneously. Experiments proved the improvement of the reference tracking ability of the DLR/HIT Hand II and the performance of the calibration and mapping of Cyberglove is verified by subjective opinions of people who have previously operated the telepresence system at DLR without the new calibration.

Acknowledgements

I would like to thank my advisor Prof. Robert Riener for his interest and the time he spared for my project, and Prof. Gerd Hirzinger for the great working environment created at DLR. I am grateful for all kinds of guidance and help of my supervisors Katharina Hertkorn and Philipp Kremer. I would also like to thank to the following people: Benedikt Pleintinger for the repairing the DLR/HIT Hand II over and over; Simon Schätzle, Moritz Maier, Conor Haines for their feedbacks on the mapping of the Cyberglove; Thomas Wimböck for sharing his experience about friction compensation; and Zhaopeng Chen for sharing his experience on the DLR/HIT Hand II.

Conventions

Throughout this thesis we use the following conventions.

Text conventions

Definitions of technical terms or short excursus are set off in coloured boxes.

EXCURSUS:
Excursus are detailed discussions of a particular point in a book, usually in an appendix, or digressions in a written text.

Definition:
Excursus

Source code and implementation symbols are written in typewriter-style text.

`myClass`

The whole thesis is written in English.

Download links are set off in coloured boxes.

File: myFile[a]

[a] http://media.informatik.rwth-aachen.de/~ACCOUNT/thesis/folder/file_number.file

Chapter 1

Introduction

This chapter introduces the motivation for doing a project on improving the matching between a robotic hand and a human hand in a telepresence system. Section 1.1—"Motivation" is followed by the introduction of the overall telepresence system which has been developed at Deutsches Zentrum für Luft- und Raumfahrt (DLR) (see Section 1.2—"The Telepresence System"). Then, hand related components of the telepresence system; namely the DLR/HIT Hand II, the latest robotic hand developed by the collaboration of DLR and Harbin Institute of Technology (HIT), and the Cyberglove®[1], a data glove, are introduced respectively in Sections 1.3—"Slave Side: DLR/HIT Hand II" and 1.4—"Master Side: Dataglove". Chapter 1—"Introduction" closes with the goal of this thesis work (see Section 1.5—"The Goal of the Thesis").

1.1 Motivation

The telepresence system developed at DLR is proposed as a possible solution to the maintenance problem of the satellites. The ever-increasing number of satellites being sent to space necessitates more operational space for proper functioning of the satellites. More operational space can be cre-

[1] http://www.cyberglovesystems.com/products/cyberglove-ii/overview Retrieved August, 2011

ated by de-orbiting the satellites which come to the end of their lifespan or maintaining the satellites with small problems. For this reason, maintenance of satellites is an important issue and it can be achieved by robotic on-orbit servicing (OOS) [Landzettel et al., 2006].

In space missions like on-orbit servicing, one is bounded by the distance and hazardous environments barriers. Telerobotic systems can help us overcome these barriers by enabling us to perform manipulation tasks from remote locations [Preusche et al., 2005]. In 1993, ROTEX, a multisensory robot, was teleoperated by astronauts and from ground via human operators. ROTEX became the first robot to perform several task in space and it had proven the usefulness of the concept [Hirzinger et al., 1994].

A telepresence system is a particular case of telerobotic systems. In a telepresence system, a human operator is included in the control loop both as the high-level decision maker and as a part of the control, e.g by adjusting forces exerted on manipulated objects. The operator interacts with the master side of the telepresence system and the manipulation task is performed via the slave side. In such a system, the level of immersion is supposed to be high, so the remote manipulator should be interpreted as a natural extension of the operator's body [Preusche et al., 2005]. High level of immersion is achieved by coupling the movements of the human operator and the teleoperator, and providing feedback to the human operator about the state of the remote location through a fast communication link. Stoll et al. [2009] classified telerobotic systems that provide on-orbit servicing as transparent telepresence, telepresence, and telerobotic systems. This classification depends on the communication delays. They should be less than 0.1 sfor transparent telepresence, less than 1 sfor telepresence, and less than 10 sfor telerobotics. According to this classification, the Robotic Component Verification aboard the ISS (Rokviss) [Landzettel et al., 2006] is so far the only on-orbit servicing system that can achieve transparent telepresence. Besides, SMART Orbital Life Extension Vehicle (SMART-OLEV) [Tarabini et al., 2007] and the Deutsche Orbitale Servicing Mission (DEOS) [Sommer, 2004] are two OOS systems that are planned to be implemented in the future. These two systems will be able to achieve telepresence

[Stoll et al., 2009].

In order to achieve a high level of immersion, providing instantaneous feedback to a human operator who uses a telepresence system is crucial, but not sufficient. A telepresence system should also ensure that the coupling between the movements of the human operator and the teleoperator are intuitive, in other words the both sides' movements should be matched to one another. In this work, it is attempted to improve the human operator's experience and ease of use while using a telepresence system, which uses an anthropomorphic robotic hand as a manipulator. For this purpose, the matching between a robotic hand and a human hand is improved by improving a robotics hands ability to follow given references and the mapping between a robotic hand and a human hand.

MASTER SIDE OF A TELEPRESENCE SYSTEM:
a medium for acquiring the operator commands and feeding back the data acquired by the remotely operating robot.

Definition: *Master side of a telepresence system*

SLAVE SIDE OF A TELEPRESENCE SYSTEM:
a remotely operating robot which replicates the movements of the operator and senses the environment for the operator.

Definition: *Slave side of a telepresence system*

For humans, hands have critical importance in manipulation tasks. The Greek philosopher Anaxagoras[2] claimed that the reason why humans are so distinguished from other animals is the ability to use their hands. On the other hand, later Aristotle[3] claimed that the relation is the other way around, i.e. it is our high cognitive capabilities that made our hands so useful. Whether one agrees with Anaxagoras or with Aristotle, it is unarguable that hands are the major manipulation organs of the human-beings,

[2] Anaxagoras (500 BC - 428 BC) was a Pre-Socratic Greek philosopher. Anaxagoras was the first philosopher to bring philosophy from Ionia to Athens [Wikipedia, 2011a].

[3] Aristotle (384 BC - 322 BC) was a Greek philosopher, a student of Plato and teacher of Alexander the Great. Together with Plato and Socrates (Plato's teacher), Aristotle is one of the most important founding figures in Western philosophy [Wikipedia, 2011b].

and they are closely linked to the high cognitive abilities of humankind. So, if a telepresence system incorporates an anthropomorphic robotic hand, better matching of the robotic hand functions with the human hand's would possibly result in higher level of immersion and better performance in manipulation [Bicchi, 2000].

In the next section, the telepresence system used in this work is briefly introduced, and in Sections 1.3 and 1.4, more detailed descriptions of the hand related components of the telepresence system, DLR/HIT Hand II and Cyberglove®, are made. In Section 1.5, the issues that are addressed by this work are listed based on the descriptions of the hand related components of the telepresence system.

1.2 The Telepresence System

The multimodal telepresence system developed at DLR consists of three major parts: on the slave side Justin, a humanoid robot; and on the master side a Human-Machine Interface (HMI); and the communication channels (see Figure 1.1). Users can attach themselves to the HMI by putting their hands into the handles at the end effectors of two Light Weight Robots[4]. The Light Weight Robots measure the positions from the master side and send them as references to Justin, and in the meantime apply haptic feedback to the master side. The finger movements of the user are coupled with the fingers of the DLR/HIT Hand II, which is attached to the end of Justin's arms, using the Cyberglove®,, a data glove, used for tracking the finger positions of the human (see Figure 1.2). While using the telepresence system, the users also wear a head mounted display. This display provides the user with 3D images acquired by the stereo cameras mounted on Justin's head. There are visual markers on this head mounted display

[4]DLR Light Weight Robot III is developed at DLR Institute of Robotics and Mechatronics, has a "load to weight ratio of at least 1:1. Similar to a human arm the robot has seven degrees of freedom. Each joint is equipped with a motor position sensor, a joint position sensor and a joint torque sensor." [DLR-Website, 2011b]. http://www.dlr.de/rm/desktopdefault.aspx/tabid-3803/6175_read-8963/ Date accessed 24 August 2011.

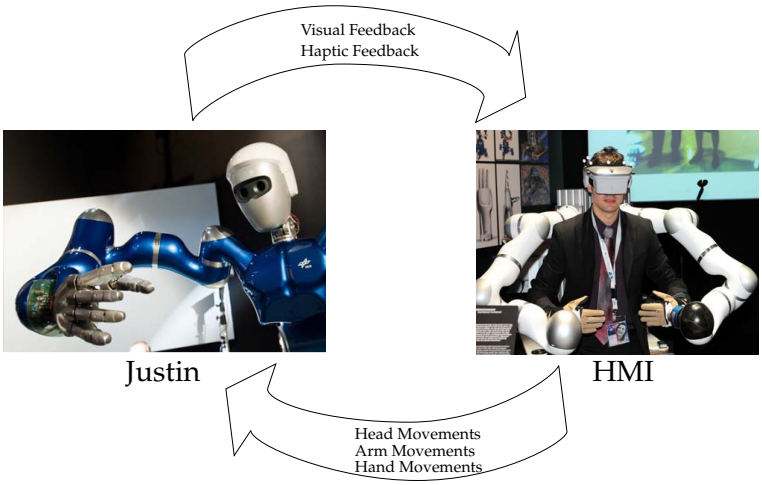

Figure 1.1: The telepresence system

which are tracked by cameras and provide reference for the Justin's head movement. Tracking of the head movements gives the user the ability to look around the surrounding as if being present at the remote location. The communication is responsible of carrying the movement and feedback information between the HMI and remotely located Justin.

Figure 1.2: Cyberglove together with the handle of the HMI

1.3 Slave Side: DLR/HIT Hand II

The DLR/HIT Hand II is a five-finger dexterous hand (see Figure 1.3) with 15 degrees of freedom (DOF); and joint torque, position, and temperature sensing. Every finger of the hand is identical and has three actuated DOF. There is no DOF for the palm movement, but when used with the HMI, the palm movement of the user is also restricted because of the handles of the HMI (see Figures 1.2 and 1.4).

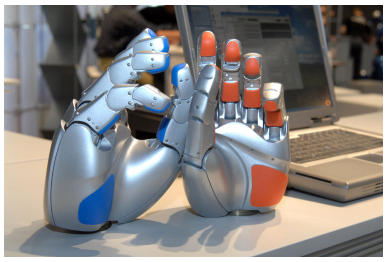

Figure 1.3: DLR/HIT Hand II [DLR-Website, 2011a]

Each individual finger incorporates the required electronic and mechanical components on itself. This is a clear advantage of the DLR/HIT Hand II [Liu et al., 2008].

Figure 1.4: Cyberglove together with the HMI

Two of the degrees of freedoms of each finger achieve the flexion/extension and abduction/adduction movements at the metacarpophalangeal joint and the last degree of freedom is used to control the motion of the proximal and distal interphalangeal joints. Two mechanically coupled brushless DC motors, Maxon EC20 flat, are used to control the abduction θ_{abd} and flexion angles θ_{flex} at the metacarpophalangeal joint. The proximal and distal interphalangeal joints are coupled by a wire tendon with $1:1$ ratio and their angle θ_{dist} is controlled with a single brushless DC motor of the same type. The relations between θ_{dist}, θ_{abd}, θ_{flex} and motor angles q_1, q_2, q_3 are given in Equations 1.1, 1.2 and 1.3.

$$\theta_{\text{dist}} = q_1 \tag{1.1}$$

$$\theta_{\text{abd}} = \frac{q_2 - q_3}{2}, \tag{1.2}$$

$$\theta_{\text{flex}} = \frac{q_2 + q_3}{2}, \tag{1.3}$$

The above explained mechanical coupling imposes a synchronization requirement for the motors at the metacarpophalangeal joint. If this requirement is not met, the resulting motion of the finger of interest will not resemble the commanded motion, e.g. if one of the fingers is only flexed and the two motors at the metacarpophalangeal joint do not converge to the reference at the same rate, then the resulting motion would have abduction and adduction movements, i.e. deviations from the intended movement (see Equation 1.2).

Figure 1.5: Bevel gears at the base joint

The two motors are mechanically coupled using transmission components such as harmonic drives and bevel gears (see Figure 1.5). The use of these transmission components introduces friction. This friction not only makes the control of individual motors more difficult, but also creates a further problem related to the synchronization requirement as the friction forces experienced by different motors are not necessarily the same.

1.4 Master Side: Dataglove

On the master side of the telepresence system at DLR, human hand movements are measured using a dataglove namely Cyberglove. The dataglove has 22 sensors, strain gauges (see Figure 1.6). The sensors on the dataglove have less than one degree resolution, three degrees repeatability, and 0.6% maximum nonlinearity over full joint range[5].

[5]http://www.cyberglovesystems.com/products/cyberglove-ii/specifications Retrieved August, 2011

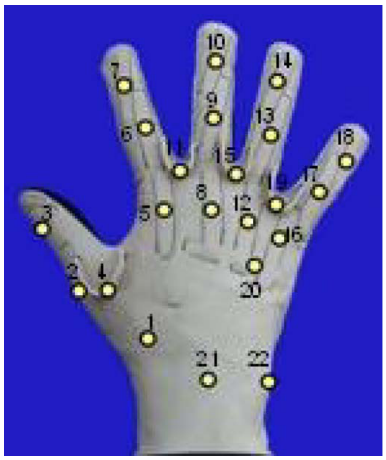

Figure 1.6: Cyberglove sensor locations [Zhou et al., 2010]. The rectangular stitches and the U-shapes are the regions where the sensors are located.

The measured hand data is transmitted to the slave side for performing manipulation tasks. Because of the sensor uncertainties like sensor drift and offset, the differences of the hand sizes among people, and the HMI handle (see Figure 1.2), which presses on some of the sensors, the dataglove needs to be calibrated.

1.5 The Goal of the Thesis

This work improves the ability of the DLR/HIT Hand II to repeat a human user's hand movements. To achieve this goal, one should first be able to measure the human hand joint angles accurately, i.e. datagloves should be accurately calibrated, and map these joint angles to the robotic hand workspace. The mapping is needed, because although being an anthropomorphic hand, DLR/HIT Hand II is not an exact match to a human hand, and the kinematics measured by the Cyberglove and the actual kinematics of the human hand do not match as well. Figure 1.6 depicts the locations of the sensors on the Cyberglove. The resulting human hand kinematics approximated by the Cyberglove is given in Figure 1.7. The human hand's kinematic model approximated by the Cyberglove's sensor configuration and

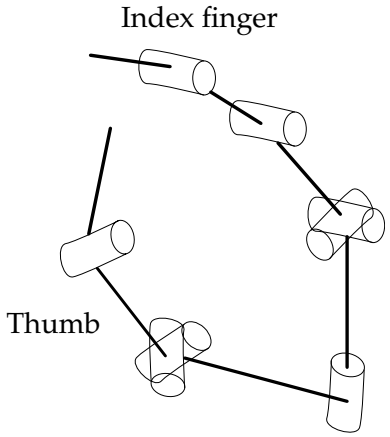

Figure 1.7: Reduced human hand kinematics measured by Cyberglove sensors - middle, ring and pinky fingers have the same kinematic structure as the index finger

the DLR/HIT Hand II's kinematic model are not the same (see Figures 1.7 and 1.8). The most obvious of the differences between the master and slave side are the extra joint of the robotic thumb, robotic hand's lack of the thumb rotation joint, coupling of the proximal and distal joints of the robotic hand and the finger segment sizes. Without taking these differences into account, they would degrade the human operator's level of perception of the robotic hand as a natural extension of his/her body. This would possibly lead to a need for more cognitive effort from the user while performing manipulation tasks in a telepresence system. In this work it is hypothesized that with a good calibration and a mapping, manipulation tasks can be made easier and more intuitive for the user. Calibrating the Cyberglove and mapping the measured human hand joint angles to robotic hand joint angles is one of the major tasks achieved in this work.

Besides the calibration of the Cyberglove and a mapping between human hand and robotic hand, accurate control of the robotic hand is another task to be fulfilled, i.e. one should also ensure that the robotic hand can accurately follow reference commands. In Section 1.3—"Slave Side: DLR/HIT Hand II", it is stated that due to the use of transmission components, the fingers of DLR/HIT Hand II experience high friction. High friction makes the accurate control of the fingers a challenge. Another control chal-

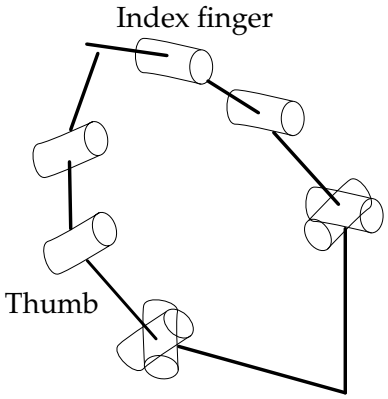

Figure 1.8: DLR/HIT Hand II kinematics - middle, ring and pinky fingers are identical to the index finger. Distal and proximal phalangeal joints are mechanically coupled with $1:1$ ratio.

lenge is the synchronization requirement explained in the same section. These are tackled by implementing a friction compensation and designing a controller that can both handle the uncertainties that are not addressed by the friction compensation and simultaneously fulfill the synchronization requirement. All the tasks that are performed to meet the requirements of the system are given in the following list.

Calibration of Remote Hand Control:

- Friction compensation (see Chapter 2)
  - choosing a friction model: although friction is a highly complex and nonlinear phenomenon, its dynamics are known up to some extent and can be modeled,
  - identifying the friction parameters of the robotic hand for the selected friction model: depending on the chosen friction model, one has to identify the parameters associated with it, so that the friction torques on the motors can be estimated.
- Controller design (see Chapter 3)
  - compensating the uncertainties of the friction that the friction model cannot capture, and other

sources of disturbances: imperfections of the friction model, change of friction parameters with change of temperature and the differences of the friction characteristics depending on the joint positions are some of the uncertainties that should be taken care of,

- achieving the synchronization of the mechanically coupled motors.

- Calibration and mapping of the Cyberglove (see Chapter 4)
  - calibrating the data glove sensors,
  - making a mapping between the human hand and the robotic hand.

Chapter 2

Friction Compensation

High friction of the base joint of the DLR/HIT Hand II makes the control of the flexion and abduction movements difficult (see Section 1.3—"Slave Side: DLR/HIT Hand II"). A possible remedy of the high friction problem is the estimation and compensation of the friction torques based on an appropriate friction model. For controlling systems with friction, several studies used friction models [Canudas-de Wit et al., 1995], [Lee and Tomizuka, 1996], [Le Tien et al., 2008]. In the next section, their different approaches for compensating the friction are introduced; Canudas-de Wit et al. only focused on the estimation according to the friction model, while Lee and Tomizuka and Le Tien et al. used disturbance observers alongside the friction models. Although both Lee and Tomizuka and Le Tien et al. used disturbance observers, they had used the observers in different ways. Unlike the regular disturbance observer used in the former of the two studies, in the latter study a disturbance observer which observes only the friction based on the chosen model, was designed and used.

After the introduction of these studies, the choice of the friction model is explained in Section 2.1.1—"Possible Friction Models". Depending on the choice of the friction model, new parameters that define the friction characteristics of the joints, need to be determined. A method for identifying these parameters is needed, because for each different finger of DLR/HIT Hand II, the respective friction charac-

teristics are dramatically different. This difference makes use of a set of nominal values impossible. In Section 2.1.2—"Parameter Identification for a Friction Model" a previous work on friction parameter identification is explained and then, the identification routine implemented in this work is introduced in Sections 2.2.1—"Parameter Identification Routine" and 2.2.2—"A Graphical User Interface for the Identification of the Friction Parameters".

2.1 Related Work

As stated in the previous section, Canudas-de Wit et al. [1995]; Lee and Tomizuka [1996]; Le Tien et al. [2008] use different methods for estimating and eventually compensating the friction.

Canudas-de Wit et al. proposed a friction model as an extension to the Dahl Model [Dahl, 1968] and tried to identify the dynamic friction acting on a servo-system as a function of measured velocities. The Dahl Model assumes that the relation between friction force and position is analogous to a stress-strain curve with hysteresis. Unlike the Coulomb friction, the Dahl Model is not discontinuous. Although the Dahl Model can explain the spring-like behavior during stiction, it does not include the stiction force, i.e. high friction forces close to zero velocity, [Canudas-de Wit et al., 1995]. Canudas-de Wit et al.'s extension includes the stiction forces to the Dahl Model. The estimated friction obtained from the proposed model was used together with a second-order observer, a PID controller, and a feedforward term for the nominal inertia of system. On the one hand, the design is able to drive the observer error asymptotically to zero with the assumption that the parameters of the friction model are known. On the other hand, the authors warn that this is a strong assumption, and the sensitivity of the results to this assumption had not been investigated [Canudas-de Wit et al., 1995].

Lee and Tomizuka used a simpler model with respect to the one proposed by Canudas-de Wit et al.. Their model combines the viscous friction, stiction and Coulomb friction. A

friction compensator based on this model was used alongside a control scheme which has three components: namely, a PD controller at position level; a zero phase error tracking controller (ZPETC) as a feedforward controller; and a disturbance observer (DOB) at velocity level. They compared the performance of the proposed controller with ZPETC combined with a PD controller with and without a friction compensator, which compensates for the estimated friction given by the chosen model. Their results favored the DOB as the best of the compared controllers. It should be noted that the friction compensator used in Lee and Tomizuka, unlike Canudas-de Wit et al., depends on the derivative of the reference trajectory, instead of the measured velocities. Lee and Tomizuka claimed that this feedforward approach for friction compensation improves the tracking performance [Lee and Tomizuka, 1996].

Le Tien et al. used even a simpler friction model, which combines viscous friction and Coulomb friction. Like Lee and Tomizuka did, Le Tien et al. also used a DOB, but only to estimate the friction part of the disturbance torque. Together with a multi-input-multi-output (MIMO) controller, this compensation method was compared with no friction compensation and model-based friction compensation cases on the DLR medical robot, which has joint torque sensing. The controller with the friction observer resulted in best performance among the three [Le Tien et al., 2008]. Le Tien et al. listed the advantages of their approach as the avoidance of saturation or overflow of the integrate behavior of the disturbance observer under external disturbance torque, the possibility to use it together with impedance control in contact with the environment, the ease of design because of its independence from the MIMO controller design, and finally the global asymptotic stability of the original MIMO controller even in the presence of friction. The only limitation reported is the overcompensation to overcome stiction. As a possible solution, Le Tien et al. proposed monitoring energy corresponding to friction and friction compensation, and switching off or scaling down the friction compensation in case energy exceeds a certain positive threshold.

2.1.1 Possible Friction Models

In the previous section, several studies that differently deal with the friction compensation problem are introduced. However, the friction literature is not limited to these models. Olsson et al. [1998] made a very good survey on friction models. They are classified as static and dynamic models. Although, Olsson et al. favored the use of dynamic models, for the sake of simplicity, only static models are considered in this work (see Figure 2.1). The main reason for selecting simpler models is the necessity of a routine for identifying the unknown friction parameters (see Section 2—"Friction Compensation"). As the complexity of the friction model increases, the identification of parameters becomes more difficult. Because the friction characteristics that dynamic models can reflect, do not appear under constant velocity experiments, the fingers need to be moved at a wide range of velocities and accelerations [Olsson et al., 1998]. Due to the high friction characteristics of the DLR/HIT Hand II, moving the motors at the base joint with the required velocity or acceleration profile is almost impossible. Also, the change in the friction properties under different conditions like temperature or location, and the errors in the parameter estimation make a more complicated model less favorable. To sum up, although dynamic models contain more information on the friction phenomenon, they are not feasible in this case and the possible choices of the friction model is limited to the static models. Mathematical representations of the possible choices; Coulomb friction τ_c, viscous friction τ_v, combination of the Coulomb and viscous frictions $\tau_{\mathrm{c+v}}$ and the Stribeck friction τ_S, are given by the following equations:

$$\tau_c = c\,\mathrm{sign}(\dot{q}) \tag{2.1}$$

$$\tau_v = b\dot{q} \tag{2.2}$$

$$\tau_{\mathrm{c+v}} = b\dot{q} + c\,\mathrm{sign}(\dot{q}) \tag{2.3}$$

$$\tau_S = \tau_{\mathrm{c+v}} + \mathrm{sign}(\dot{q})(\tau_s - c)e^{-c_w|\dot{q}|} \tag{2.4}$$

where τ_s is the stiction torque; $\dot{q}$ is the angular velocity; and the Coulomb friction coefficient c, the viscous friction coefficient b, and the stiction coefficient c_w are the unknown parameters that need identification.

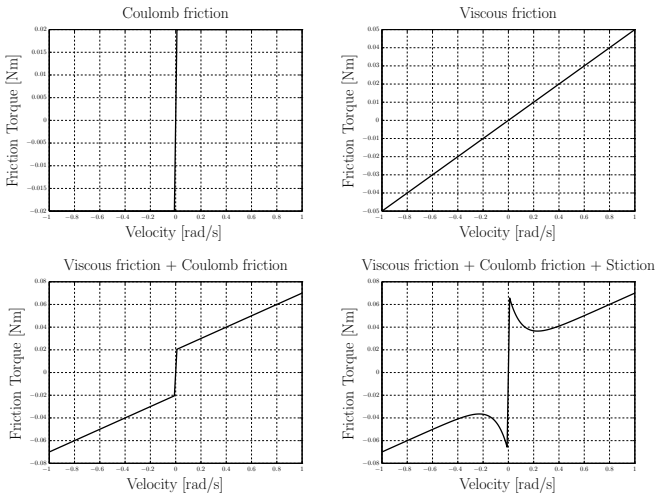

Figure 2.1: Candidate friction models

Among the static models, the Stribeck model, which combines the Coulomb, viscous and stiction phenomena, also requires operation at low velocities in order to be able to identify the stiction related parameters (see Figure 2.1). The model that combines viscous friction and Coulomb friction, is the most detailed model whose parameters can be estimated relatively easily. This model is chosen as the friction compensation model, and the friction phenomena that are not addressed by this model, are decided to be handled by the controller design.

2.1.2 Parameter Identification for a Friction Model

For the identification of the friction parameters of the chosen model, a previous work [Connette, 2006] on the calibration of the DLR Hand II is used as a guideline, and is shortly described here. According to this previous work, the dynamics concerning a motor is given by Equation 2.5 where the friction is modeled as the sum of Coulomb and viscous frictions. To be able to identify the Coulomb friction term c and the viscous friction coefficient b, the motors are moved at several different velocities for a predefined time window: nN samples. The duration of every velocity level, in other words the number of samples N, is kept

the same, so that equal amount of data is collected for each of the n velocity levels; therefore, their weights in the fitting are also kept equal. Because the hand used in Connette's work lacks velocity sensors motor position values q are recorded during the data collection phase. The recorded position values are then used to obtain the resulting motor velocities $\dot{q}$. Using the resulting velocities, Equation 2.5 is solved for the parameters c and b, and the inertia I with a least-squares method:

$$I\ddot{q} = \tau - b\dot{q} - c\,\mathrm{sign}(\dot{q}). \tag{2.5}$$

In order to convert Equation 2.5 into a form that can be used for a least-squares estimation, first all estimation parameters are moved to the left side of the equation. The resulting equation

$$I\ddot{q} + b\dot{q} + c\,\mathrm{sign}(\dot{q}) = \tau \tag{2.6}$$

is then multiplied by $\dot{q}$ on both sides, so that one can replace the sign function with the absolute value (see Equation 2.7).

$$I\dot{q}\ddot{q} + b\dot{q}^2 + c\underbrace{\dot{q}\,\mathrm{sign}(\dot{q})}_{|\dot{q}|} = \dot{q}\tau \tag{2.7}$$

By integrating Equation 2.7 over one time step using a trapezoidal approximation, Equation 2.5 is discretized and written as a function of the velocity $\dot{q}$:

$$\begin{aligned}(\dot{q}_{k+1}^2 - \dot{q}_k^2)I + t_s(\dot{q}_{k+1}^2 + \dot{q}_k^2)b + t_s(\dot{q}_{k+1} + \dot{q}_k)c \\ = ts(\tau_{k+1}\dot{q}_{k+1} + \tau_k\dot{q}_k)\end{aligned} \tag{2.8}$$

where $k = 0 \cdots nN, k \in \mathbb{N}$.

$$\underbrace{\begin{bmatrix} \frac{1}{2}(\dot{q}_{k+1}^2 - \dot{q}_k^2) & \frac{t_s}{2}(\dot{q}_{k+1}^2 + \dot{q}_k^2) & \frac{t_s}{2}(\dot{q}_{k+1} + \dot{q}_k) \\ & \vdots & \end{bmatrix}}_{LS \in \mathbb{R}^{nN \times 3}} \begin{bmatrix} I \\ b \\ c \end{bmatrix}_{3\times 1} = \begin{bmatrix} \frac{t_s}{2}(\tau_{k+1}\dot{q}_{k+1} + \tau_k \dot{q}_k) \\ \vdots \end{bmatrix}_{nN\times 1} \quad (2.9)$$

Finally, the parameters I, b, and c are solved by multiplying both sides of Equation 2.8 by $LS^\dagger \in \mathbb{R}^{3\times nN}$, which is the Moore-Penrose pseudoinverse of LS (see Equation 2.10).

$$\begin{bmatrix} I \\ b \\ c \end{bmatrix} = LS^\dagger \begin{bmatrix} \frac{ts}{2}(\tau_{k+1}\dot{q}_{k+1} + \tau_k \dot{q}_k) \\ \vdots \end{bmatrix}. \quad (2.10)$$

This approach resulted in high condition numbers of the fitting matrices, i.e. matrices are ill-conditioned (see Table 2.1). The number of estimation variables are reduced to two by fixing the value of either I or c. This led to lower condition numbers, the former leading to even lower condition numbers (see Tables 2.2 and 2.3). The reason why fixing I resulted in lower condition numbers is possibly the small amount of samples collected while acceleration takes place. Since the total duration of movements with a constant velocity command is significantly larger than the total duration of movements with acceleration, the effect of I on the least-squares fitting is insignificant. In other words, for a relatively large range of I values, least-squares fitting of the same data set will lead to similar b, and c values. Note that the variations of the estimated b and c values are very little between the cases that I is also estimated and it is fixed (see Tables 2.1 and 2.3). Because of that reason, for the rest of this work, the parameter identification routine is used by fixing I.

	I [kg m^2]	b [kg m^2/s]	c [kg m^2/s^2]	condition of LS
Motor 1	4.96×10^{-4}	0.1484	-0.0552	1047.7
Motor 2	6.79×10^{-4}	0.1555	-0.0322	852.75
Motor 3	7.57×10^{-4}	0.1102	0.00389	630.86

Table 2.1: Estimation results of Connette [2006] for no fixed parameter case

	I [kg m^2]	b [kg m^2/s]	c [kg m^2/s^2]	condition of LS
Motor 1	4.96×10^{-4}	0.1385	set to 0	51.15
Motor 2	6.79×10^{-4}	0.1494	set to 0	42.27
Motor 3	7.57×10^{-4}	0.1108	set to 0	33.80

Table 2.2: Estimation results of Connette [2006] for fixed c

Definition:
Condition number

CONDITION NUMBER:
"the ratio C of the largest to smallest singular value in the singular value decomposition of a matrix. A system is said to be singular if the condition number is infinite, and ill-conditioned if it is too large" [Lichtblau and Weisstein, 2011].

In Connette's report, it is stated that this estimation of the friction is not satisfactory as the friction parameters became negative. Besides, two other possible reasons of unsatisfactory behavior are the change of the parameters, such as temperature, during operation; and the unmodeled dynamics of the friction. The friction model used by Connette is decided to be used in this work as the starting model because of its simplicity and the control challenges that prevent using more involved friction models. The friction phenomena which are not covered by this model are addressed with the control (see Section 3—"Controller Design").

	I [kg m^2]	b [kg m^2/s]	c [kg m^2/s^2]	condition of LS
Motor 1	set to 10^{-3}	0.1484	-0.0554	20.81
Motor 2	set to 10^{-3}	0.1555	-0.0327	20.523
Motor 3	set to 10^{-3}	0.1102	0.00386	18.875

Table 2.3: Estimation results of Connette [2006] for fixed I

	I [kg m^2]	b [kg m^2/s]	c [kg m^2/s^2]	condition of LS
Motor 2	set to 2×10^{-3}	0.3004	0.4939	9.7257
Motor 3	set to 2×10^{-3}	0.3522	0.6602	9.2592

Table 2.4: Estimation results for DLR/HIT Hand II with Connette [2006]'s routine using τ_{est} and a nominal value of I

2.2 Own Work

In the following sections, the changes to Connette's work and the details of the generic GUI are explained. Connette's friction parameter identification routine is improved and implemented with a generic Matlab Graphical User Interface (GUI) that automates the data collection for parameter identification and computes the estimated friction parameters. The new routine is compared to Connette's routine and it is shown that both the sum of the least-squares errors and the condition numbers are reduced.

2.2.1 Parameter Identification Routine

The above explained parameter identification routine needs torque measurements at the motors, whereas the torque sensors of the DLR/HIT Hand II are located at the joints. The main source of the friction is the transmission components between the motors and the base joint. Because of this reason, the new model uses the estimated motor torques instead of the measured ones. The motor torques are estimated using the commanded pulse-widths u_{PWM} (see Equation 2.11), and these commanded values are scaled by the torque constant K_t (see Equation 2.12). After this change, both physically appropriate and repeatable friction models are obtained (see Figures 2.2 and 2.3).

$$\tau_{est} = K_t u_{PWM} \tag{2.11}$$

$$I\ddot{q} = \tau_{\text{est}} - b\dot{q} - c\,\text{sign}(\dot{q}) \tag{2.12}$$

	I [kg m^2]	b [kg m^2/s]	c [kg m^2/s^2]	condition of LS
Motor 2	set to 2×10^{-3}	0.39	0.3241	4.5215
Motor 3	set to 2×10^{-3}	0.4243	0.5344	4.0482

Table 2.5: Estimation results for DLR/HIT Hand II with the new routine using τ_{est} and a nominal value of I

A further modification to the procedure used by Connette, is using the approximated dynamics given by Equation 2.12 without manipulating it, i.e. keeping the sign and avoiding the trapezoidal approximation. By using the trapezoidal integral approximation, noise that would stem from the numerical differentiation of the velocity was aimed to be eliminated, but this approach introduces a residual error as the least-squares estimation is not anymore made for the actual measurement data, but for the average of the two consecutive measurement data (see Equation 2.8). Instead of using the trapezoidal integral approximation, numerical differentiation of the velocity is used to construct LS_{new}, which replaces LS (see Equation 2.13). As previously stated, accelerations become significant for a very short duration during the data gathering phase, so the noise introduced by numerical differentiation is not so significant. The results show that with this approach not only the sum of squared estimation errors are reduced (see Figures 5.1 and 5.2 in Section 5.2), but also the condition numbers are improved, i.e. lower condition numbers are achieved (see Tables 2.4, 2.5 and Figures 2.2, 2.3).

$$\underbrace{\begin{bmatrix} \dot{q}_k & \operatorname{sign}(\dot{q}_k) \\ \vdots & \vdots \end{bmatrix}}_{LS_{\text{new}} \in \mathbb{R}^{nN \times 2}} \begin{bmatrix} b \\ c \end{bmatrix}_{2\times 1} = \begin{bmatrix} \tau_{\text{est},_k} - I\ddot{q}_k \\ \vdots \end{bmatrix}_{nN\times 1}. \quad (2.13)$$

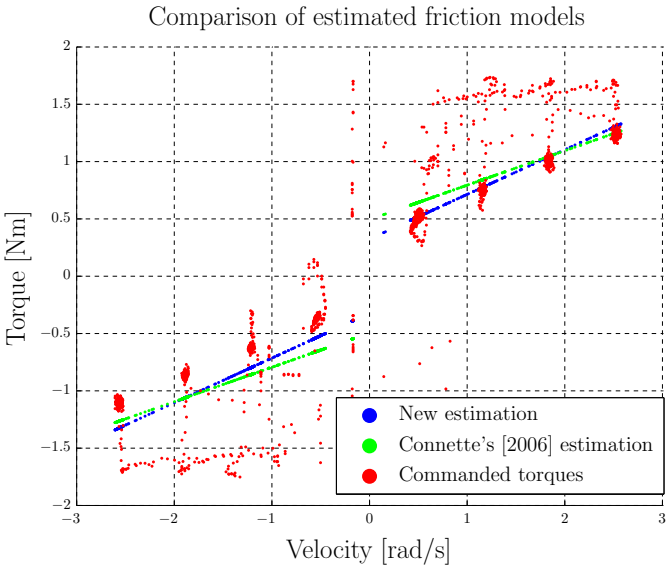

Figure 2.2: Comparison of the new friction parameter estimation and Connette [2006] friction parameter estimation for the 2^{nd} motor of the thumb using experiment data recorded for the DLR/HIT Hand II

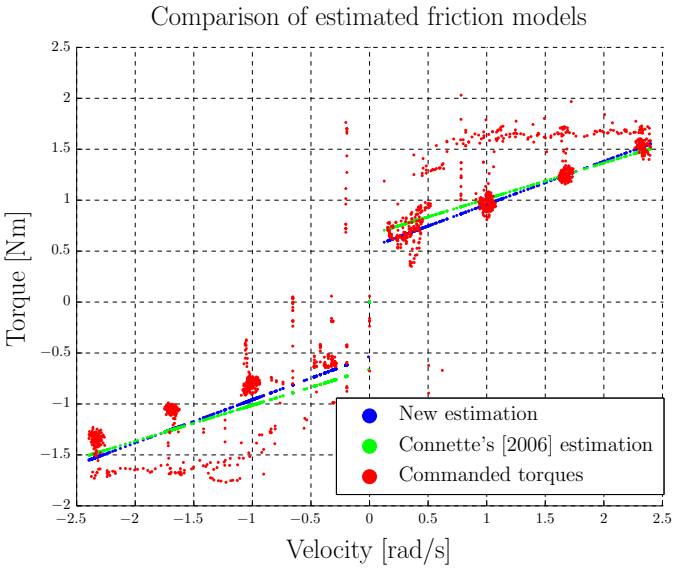

Figure 2.3: Comparison of the new friction parameter estimation and Connette [2006] friction parameter estimation for the 3^{rd} motor of the thumb using experiment data recorded for the DLR/HIT Hand II

2.2.2 A Graphical User Interface for the Identification of the Friction Parameters

A generic Matlab GUI (see Figure 2.4) and a Simulink state machine is built for automating the friction identification routine that is introduced here. Using the Matlab GUI, a user can connect to (or disconnect from) the real-time computer running the Simulink model, select the hand and the finger for identifying its friction parameters, load previously estimated friction parameters, or start the identification routine for the selected finger.

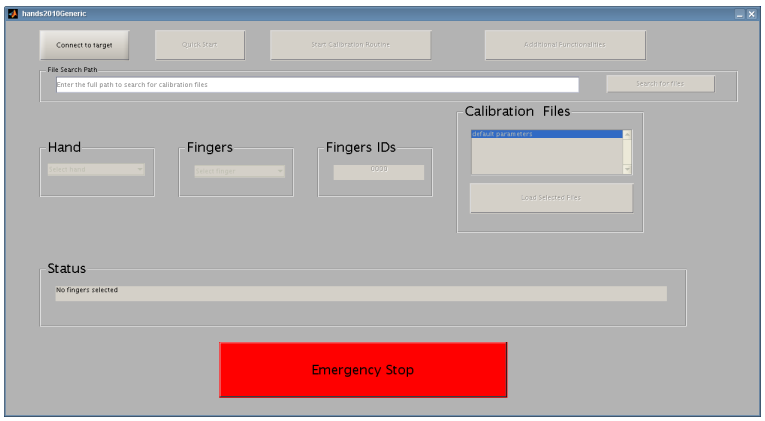

Figure 2.4: Matlab GUI for parameter identification routine

Once the identification routine is started, the user is guided through several steps. First, the user is asked to move the motors of the finger to their hardware limits one by one (see Appendix A—"A Matlab GUI for Friction Parameter Identification"). The motor limits are stored, so that the data collection can be performed over the whole workspace of the motors. The data from the whole workspace can be used for the identification of friction parameters. Due to sensor drift, the motor limits need to be determined for every run of the identification routine. It is ensured that the user moves only the right motor by leaving the motor of interest free and activating rigid position controllers for the remaining motors. After determining the limits of all motors of the selected finger, the maximum motor velocities that would span the motors' workspaces ($\pm 3 \mathrm{degrees}$ safety margin) within a predefined time window, are computed. For each motor of the selected finger four velocity levels are

chosen as 25%, 50%, 75% and 100% of the maximum velocities of the corresponding motors. Then, the GUI asks the user to confirm the initiation of the finger movement phase and starts the Simulink state machine upon user confirmation. During the finger movement phase, the state machine selects the motors one by one and sends PWM commands using a velocity level PD controller for the duration of the predefined time window for each velocity level. The velocity measurements and the PWM commands are stored in the memory of the real-time computer. After this procedure is complete, the Matlab GUI retrieves the stored data and computes the friction parameters using Equation 2.13.

In Section 5.2—"Friction Compensation", the errors of the friction torque estimation and the repeatability of the friction parameters, which are obtained by the Matlab GUI, are discussed. Also, the outputs of the friction module are compared to the outputs of a disturbance observer under different disturbance cases. Whereas in Section 5.3—"Comparison of a Disturbance Observer Based Functional Controller with a PD Controller", the friction module's effect on the controller performance is discussed.

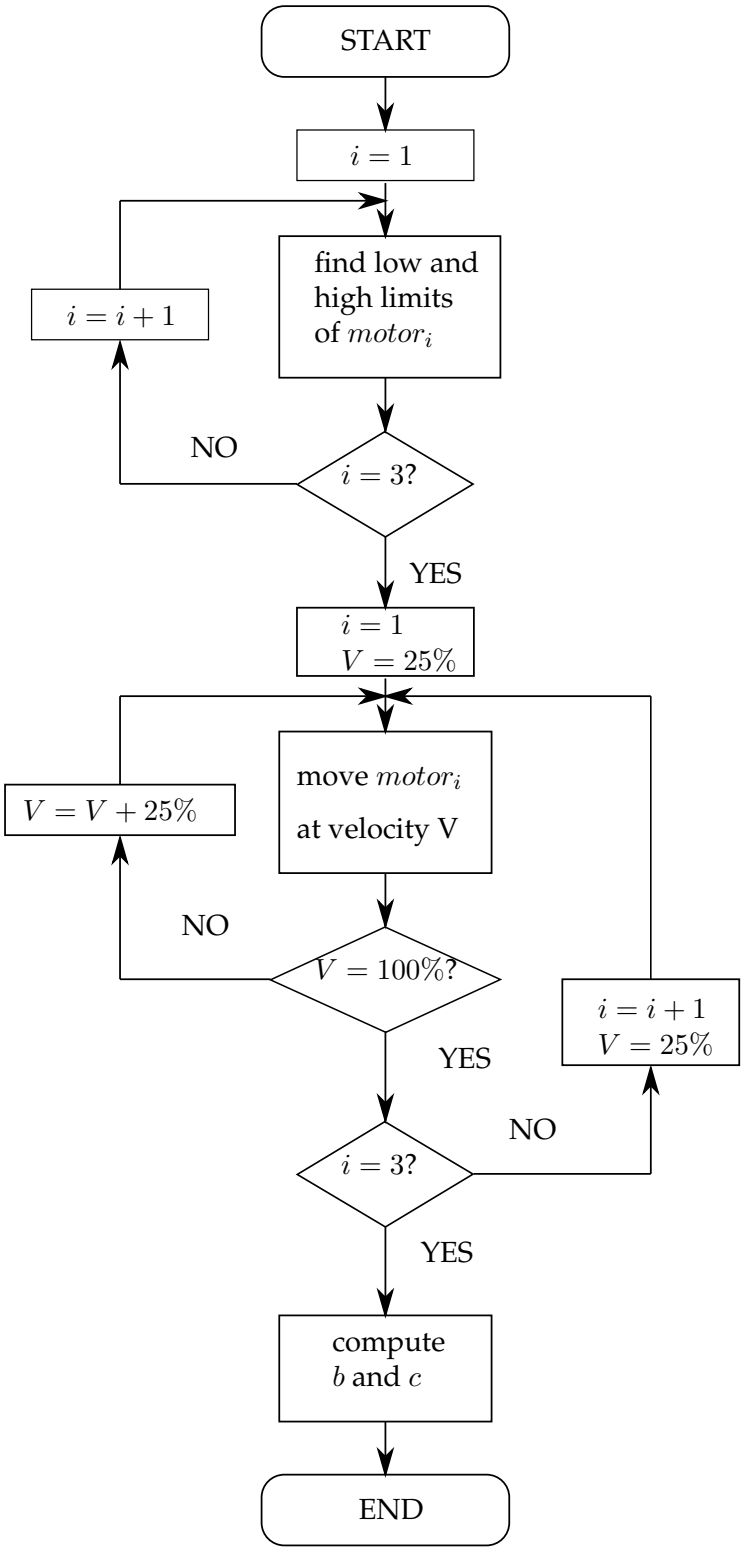

Figure 2.5: Flowchart of parameter identification routine

Chapter 3

Controller Design

The robotic hand used in this work, the DLR/HIT Hand II, has high friction at the base joint. Although a friction compensation module is implemented, the module cannot cover all aspects of the actual friction. Also, two mechanically coupled motors at the base joint need to be synchronized in order to be able to achieve the desired references (see Section 1.3). Due to these robotic hand related reasons, the controller designed for the purposes of this work should be able to synchronize the two motors and it should be robust against friction. In addition, independent of the robotic hand used, the controller should be compliant since the robotic hands are used for manipulating object.

The functionally related systems framework allows virtually decoupling coupled systems, so the synchronization can be achieved inherently by appropriately defining the functions. Also, the controllers designed according to this framework are robust against disturbances as they use disturbance observers for achieving desired dynamics.

The robotic hand related requirements are achieved with designing a controller according to the functionally related systems framework. The designed controller has compliance as an addition to the general framework. This section explains the framework, the implementation of a control scheme according to this framework (see Section 3.1), and the realization in this work (see Section 3.2) .

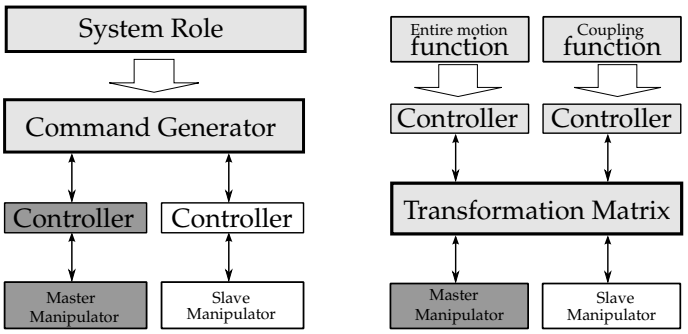

(a) Conventional bilateral system **(b)** Functional bilateral system

Figure 3.1: Design framework of bilateral system [Tsuji et al., 2006]

3.1 Related Work

The idea of functionality is proposed by Tsuji et al. [2006] for implementing adjustable bilateral control systems. Tsuji et al. [2006] define *function* "as a minimum component of a *system role*", where *system role* "is a description of the requirement from a user to a robot control system". In a conventional bilateral system, the *system role* and controllers are associated to one another through a command generator (see Figure 3.1a). The command generator is the only link between the controllers and the system role. Individual controllers control individual actuators depending on the inputs received by the command generator and they do not guarantee achieving the system role. In order to be able to achieve the system role, the command generator needs to be designed according to the desired role and the knowledge of the designer about the dynamics of the system. On the other hand, the framework proposed by Tsuji et al. [2006] divides the system role into functions and the corresponding functions are controlled individually (see Figure 3.1b). This makes the controller design simple and explicit [Tsuji et al., 2007].

The functionally related systems framework allowed Tsuji et al. [2006] to implement different types of couplings of master and slave sides of a bilateral control system (see Figures 3.3a and 3.3b), and different motion functions for the entire system like friction compensation or inertia ma-

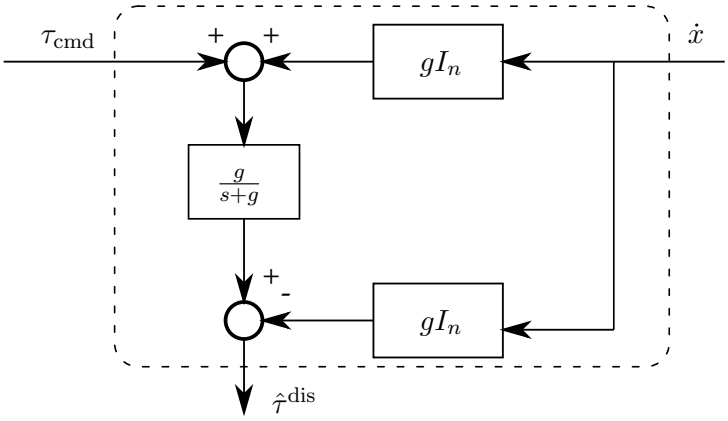

Figure 3.2: Disturbance observer [Tsuji et al., 2006]

nipulation (see Figure 3.3d). Tsuji et al. [2006] used a disturbance observer (see Figure 3.2) together with a PD controller: not for realizing the functional relation, but instead to achieve rigid coupling. The disturbance observer gets the commanded torque τ_{cmd} and the velocity $\dot{x}$ and estimates the disturbance torque $\hat{\tau}^{\text{dis}}$ by using a low-pass filter with cut-off frequency g. By subtracting the unfiltered velocity signal from the filtered one, one can differentiate the velocity signal, i.e. obtain a filtered acceleration (see Equations 3.1 to 3.4). This acceleration signal is multiplied by the nominal inertia I_n to get a nominal torque signal. Finally, the estimated disturbance torque is computed as the filtered difference of the commanded torque and the nominal torque.

$$\hat{\tau}^{\text{dis}} = \frac{g}{s+g}\left(\tau_{\text{cmd}} + \dot{x} I_n g\right) - \dot{x} I_n g \tag{3.1}$$

$$\hat{\tau}^{\text{dis}} = \frac{g}{s+g}\tau_{\text{cmd}} - \left(1 - \frac{g}{s+g}\right)\dot{x} I_n g \tag{3.2}$$

$$\hat{\tau}^{\text{dis}} = \frac{g}{s+g}\tau_{\text{cmd}} - \frac{s}{s+g}\dot{x} I_n g \tag{3.3}$$

$$\hat{\tau}^{\text{dis}} = \frac{g}{s+g}(\tau_{\text{cmd}} - \underbrace{\dot{x}s}_{\ddot{x}} I_n) \tag{3.4}$$

Tsuji et al. [2007] expanded the functionality concept for multi-DOF robots in 3D space. The expanded framework is used for implementing a grasp controller. In their work,

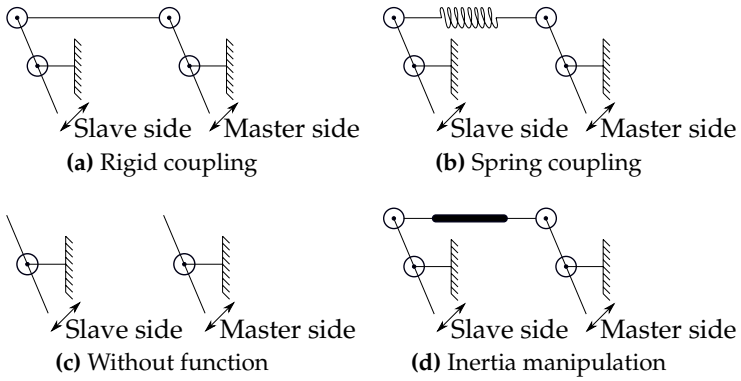

Figure 3.3: Bilateral systems with different coupling functions [Tsuji et al., 2006]

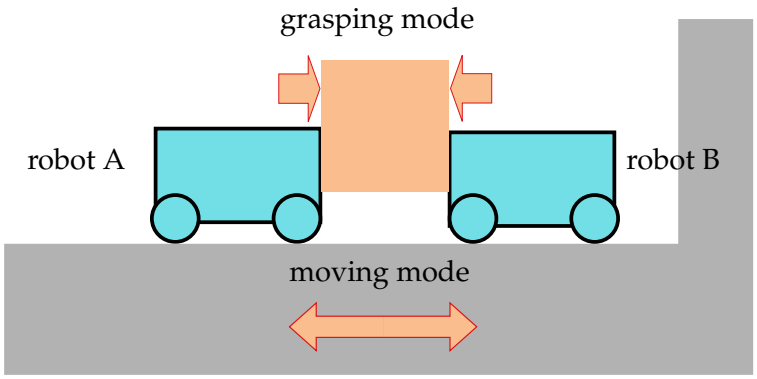

Figure 3.4: Grasping task [Tsuji et al., 2007]

Tsuji et al. [2007] break the grasping task into two functions: grasping the object, i.e. keeping two robots at a certain distance from each other, and moving the object (see Figure 3.4). The expanded framework resulted in interference of virtual dynamics of these functions. Using disturbance observers for all motors, the interference is canceled without compromising the simplicity and explicitness of the function-based controller design because function-based systems are decoupled with the disturbance observers [Tsuji et al., 2007].

A generalized functionally related systems framework is explained in detail for a system with two actuators and two functions f_1 and f_2 by Sabanovic and Ohnishi [2011]. They also explain how this framework is used to design

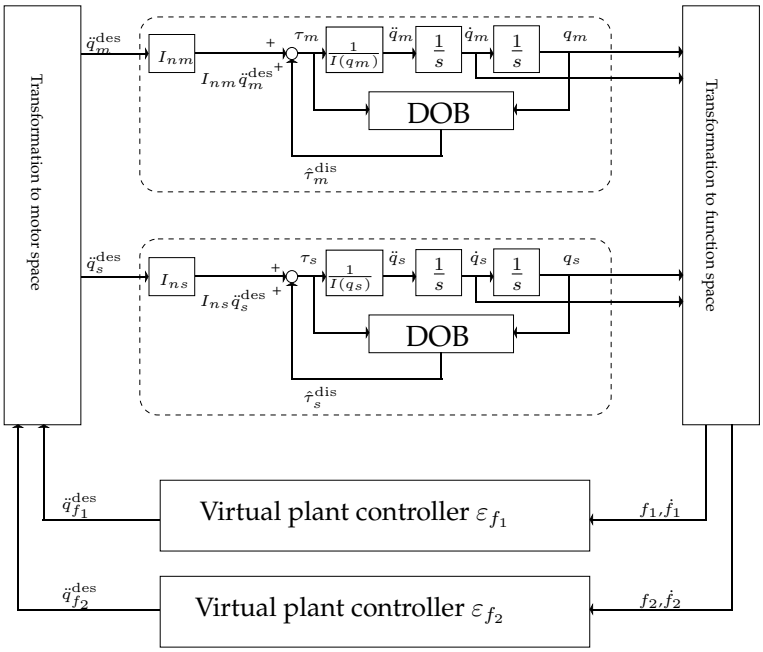

Figure 3.5: Control scheme for functionally related systems with Torque Disturbance Observer [Sabanovic and Ohnishi, 2011]

a bilateral control scheme. Figure 3.5 depicts the general control scheme where subscripts s and m refer respectively to master and slave sides. According to this scheme, first, motor angles q_s and q_m and velocities of individual motors are transformed into function space. Then, the desired accelerations that fulfill the desired dynamics of the functions are generated by virtual plant controllers in function space. The generated desired accelerations are transformed back to motor space and multiplied with the corresponding nominal inertias I_{ns} and I_{nm} to compute the desired torques for the nominal system. Lastly, the estimated disturbance torques $\hat{\tau}_s^{\text{dis}}$ and $\hat{\tau}_m^{\text{dis}}$ are added to the desired torques to generate the commanded torques τ_s and τ_m. This design assumes the following dynamics for the control system:

$$I(q_s)\ddot{q}_s = I_{ns}\ddot{q}_s^{\text{des}} + p_s \tag{3.5}$$

$$I(q_m)\ddot{q}_m = I_{nm}\ddot{q}_m^{\text{des}} + p_m, \tag{3.6}$$

where p_s and p_m are the errors in the disturbance torque estimation respectively for the slave and master sides.

In this framework, the goal is to take the two function values to zero (see Equation 3.7). This is achieved using an acceleration level control. The second time derivatives of the functions, accelerations in function space, are written in terms of the derivatives of the motor angles q_s and q_m (see Equations 3.8).

$$S_f = \{q_s, q_m : f_1(q_s, q_m) = 0 \wedge f_2(q_s, q_m) = 0\} \tag{3.7}$$

$$\begin{aligned} \ddot{f}_1 &= (c_{1s}\ddot{q}_s + c_{1m}\ddot{q}_m) + (\dot{c}_{1s})\,\dot{q}_s + (\dot{c}_{1m})\,\dot{q}_m \\ \ddot{f}_2 &= (c_{2s}\ddot{q}_s + c_{2m}\ddot{q}_m) + (\dot{c}_{2s})\,\dot{q}_s + (\dot{c}_{2m})\,\dot{q}_m \\ \text{with} \quad c_{is} &= \frac{\partial f_i}{\partial q_s}, \quad c_{im} = \frac{\partial f_i}{\partial q_m}, \quad i \in \{1, 2\} \end{aligned} \tag{3.8}$$

These acceleration terms can be decomposed into the desired accelerations $\ddot{q}_{f_1}^{\text{des}}$ and $\ddot{q}_{f_2}^{\text{des}}$ and the equivalent accelerations $\ddot{q}_{f_1}^{eq}$ and $\ddot{q}_{f_2}^{eq}$ (see Equations 3.9). After this decomposition, Equations 3.8 turns into Equations 3.10. Although the values of the functions are known and the accelerations in function space can be derived from the measured motor angles, the decomposed parts remain unknown.

$$\begin{aligned} \ddot{f}_1 &= \ddot{q}_{f_1}^{\text{des}} - \ddot{q}_{f_1}^{eq} \\ \ddot{f}_2 &= \ddot{q}_{f_2}^{\text{des}} - \ddot{q}_{f_2}^{eq} \end{aligned} \tag{3.9}$$

$$\begin{aligned} \ddot{q}_{f_1}^{\text{des}} &= \left(c_{1s}\ddot{q}_s^{\text{des}} + c_{1m}\ddot{q}_m^{\text{des}}\right) \\ \ddot{q}_{f_2}^{\text{des}} &= \left(c_{2s}\ddot{q}_s^{\text{des}} + c_{2m}\ddot{q}_m^{\text{des}}\right) \\ \ddot{q}_{f_1}^{eq} &= -(\dot{c}_{1s})\,\dot{q}_s - (\dot{c}_{1m})\,\dot{q}_m + \left(c_{1s}\frac{p_s}{I_{ns}} + c_{1m}\frac{p_m}{I_{nm}}\right) \\ \ddot{q}_{f_2}^{eq} &= -(\dot{c}_{2s})\,\dot{q}_s - (\dot{c}_{2m})\,\dot{q}_m + \left(c_{2s}\frac{p_s}{I_{ns}} + c_{2m}\frac{p_m}{I_{nm}}\right) \end{aligned} \tag{3.10}$$

These unknown parts are estimated by virtual plants. First, the dynamics of f_1 and f_2 are proposed as in Equations 3.11 where k_{ij} are positive scalars. If these dynamics are achieved, the desired accelerations can be written as in Equations 3.12. By appropriately designing virtual plants, the equivalent accelerations can be estimated by disturbance observers. Thus the desired accelerations can be determined and the desired dynamics can be achieved. An example of such a virtual plant is the one used for a bilateral system by Sabanovic and Ohnishi [2011]. This example virtual plant will be explained later in this section.

$$\begin{aligned} \ddot{f}_1(q_s, q_m) + k_{11}\dot{f}_1(q_s, q_m) + k_{12}f_1(q_s, q_m) = 0, \\ \ddot{f}_2(q_s, q_m) + k_{21}\dot{f}_2(q_s, q_m) + k_{22}f_1(q_s, q_m) = 0, \\ k_{i,j} > 0 \quad i \in \{1, 2\}, \quad j \in \{1, 2\} \end{aligned} \tag{3.11}$$

$$\begin{aligned} \ddot{q}_{f_1}^{\text{des}} &= \ddot{q}_{f_1}^{eq} - k_{11}\dot{f}_1(q_s, q_m) - k_{12}f_1(q_s, q_m) \\ \ddot{q}_{f_2}^{\text{des}} &= \ddot{q}_{f_2}^{eq} - k_{21}\dot{f}_2(q_s, q_m) - k_{22}f_1(q_s, q_m) \end{aligned} \tag{3.12}$$

The acceleration outputs generated by the virtual plants are in function space, but to control motors, these outputs should be transformed into motor space. The resulting relation between the desired accelerations in function space and the desired motor accelerations is given by Equation 3.13. To be able to transform the desired accelerations from function space to the motor space, $J_{f_1,f_2}^{s,m}$ has to be invertible (see Equation 3.14).

$$\begin{bmatrix} \ddot{q}_{f_1}^{\text{des}} \\ \ddot{q}_{f_2}^{\text{des}} \end{bmatrix} = \begin{bmatrix} c_{1s} & c_{1m} \\ c_{2s} & c_{2m} \end{bmatrix} \begin{bmatrix} \ddot{q}_s^{\text{des}} \\ \ddot{q}_m^{\text{des}} \end{bmatrix} = J_{f_1,f_2}^{s,m} \begin{bmatrix} \ddot{q}_s^{\text{des}} \\ \ddot{q}_m^{\text{des}} \end{bmatrix} \tag{3.13}$$

$$\begin{bmatrix} \ddot{q}_s^{\text{des}} \\ \ddot{q}_m^{\text{des}} \end{bmatrix} = \left(J_{f_1,f_2}^{s,m}\right)^{-1} \begin{bmatrix} \ddot{q}_{f_1}^{\text{des}} \\ \ddot{q}_{f_2}^{\text{des}} \end{bmatrix}, \quad \det\left(J_{f_1,f_2}^{s,m}\right) \neq 0 \tag{3.14}$$

One of the desired functionalities of the bilateral system design proposed by Sabanovic and Ohnishi [2011] is the position tracking of the slave side according to the reference

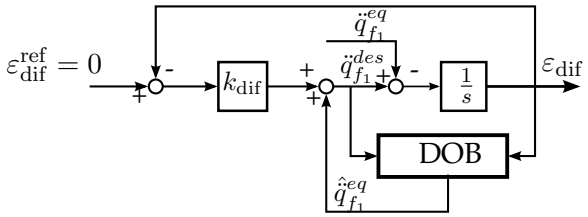

Figure 3.6: Virtual plant [Sabanovic and Ohnishi, 2011]

given by the master side. The position error of the bilateral system is defined as $\varepsilon_{qb} = q_m - q_s$. As above mentioned, a virtual plant is introduced to control the dynamics of ε_{qb}. The virtual plant controller aims to take the auxiliary error ε_{dif} to its reference $\varepsilon_{\text{dif}}^{\text{ref}} = 0$. ε_{dif} is related to ε_{qb} through Equation 3.15 where k_{qb} is a weighting scalar. By choosing a virtual plant whose dynamics are defined as an integrator (see Figure 3.6), the desired acceleration can be found. First, one can decompose the derivative of the auxiliary error ε_{dif} into the desired accelerations and the equivalent acceleration $\ddot{q}_{\text{dif}}^{eq}$ as in Equation 3.17. Then, for the chosen dynamics, one can also estimate $\ddot{q}_{\text{dif}}^{eq}$ with the disturbance observer given in Equation 3.18, where Q is a low-pass filter and g is the cut-off frequency of Q.

$$\varepsilon_{\text{dif}} = k_{qb}\varepsilon_{qb} + \dot{\varepsilon}_{qb} \tag{3.15}$$

$$\dot{\varepsilon}_{\text{dif}} = \ddot{q}_m - \ddot{q}_s + k_{qb}\dot{\varepsilon}_{qb} \tag{3.16}$$

$$\dot{\varepsilon}_{\text{dif}} = \left(\ddot{q}_m^{\text{des}} - \ddot{q}_s^{\text{des}}\right) - \ddot{q}_{\text{dif}}^{eq} = \ddot{q}_{\text{dif}}^{\text{des}} - \ddot{q}_{\text{dif}}^{eq} \tag{3.17}$$

$$\hat{\ddot{q}}_{\text{dif}}^{eq} = Q\left(\ddot{q}_{qb}^{\text{des}} + g\varepsilon_{\text{dif}}\right) - g\varepsilon_{\text{dif}} \tag{3.18}$$

One should also ensure that the obtained desired accelerations would result in the desired system behavior. The desired system behavior, hence the desired accelerations, can be produced by a system that has the desired dynamics proposed in Equation 3.11. The closed loop dynamics of the virtual plant are chosen as in Equation 3.19, i.e. a P controller with proportional gain k_{dif} (see Figure 3.6). This choice would yield to the asymptotical convergence of the closed loop dynamics to the desired dynamics (see Equation 3.20) as the estimated equivalent acceleration converges to the actual equivalent acceleration (see Equation

3.21).

$$\dot{\varepsilon}_{\mathrm{dif}} + k_{\mathrm{dif}}\varepsilon_{\mathrm{dif}} = 0 \tag{3.19}$$

$$\begin{aligned}\dot{\varepsilon}_{\mathrm{dif}} + k_{\mathrm{dif}}\varepsilon_{\mathrm{dif}} &= \frac{d}{dt}\left(k_{qb}\varepsilon_{qb} + \dot{\varepsilon}_{qb}\right) + k_{\mathrm{dif}}\left(k_{qb}\varepsilon_{qb} + \dot{\varepsilon}_{qb}\right) \\ &= \varepsilon_{qb} + \left(k_{qb} + k_{\mathrm{dif}}\right)\dot{\varepsilon}_{qb} + k_{qb}k_{\mathrm{dif}}\ddot{\varepsilon}_{qb}\end{aligned} \tag{3.20}$$

$$\dot{\varepsilon}_{\mathrm{dif}} + k_{\mathrm{dif}}\varepsilon_{\mathrm{dif}} = (1-Q)\ddot{q}_{\mathrm{dif}}^{eq} \cong 0 \tag{3.21}$$

$$\ddot{q}_{\mathrm{dif}}^{\mathrm{des}} = \hat{\ddot{q}}_{\mathrm{dif}}^{eq} - k_{\mathrm{dif}}\varepsilon_{\mathrm{dif}} \tag{3.22}$$

3.2 Own Work

In Section 1.3—"Slave Side: DLR/HIT Hand II", the relationship between the motors angles and the joint angles at the base joint of a finger of the DLR/HIT Hand II is given (see Equations 1.2 and 1.3). As earlier stated, this relationship imposes a synchronization requirement of the two motors mounted at the base joint. Synchronization is guaranteed by using the functionally related systems framework and choosing functions that would ensure the desired joint space movements:

$$f_1 = q_2 - q_3 - 2\theta_{\mathrm{abd}}^{\mathrm{ref}} = 0, \tag{3.23}$$

$$f_2 = q_2 + q_3 - 2\theta_{\mathrm{flex}}^{\mathrm{ref}} = 0. \tag{3.24}$$

Using the transformation matrix T, motor angles q_2 and q_3 are transformed into the functions f_1 and f_2 (see Equation 3.25).

$$\begin{bmatrix} f_1 \\ f_2 \end{bmatrix} = \underbrace{\begin{bmatrix} 1 & -1 \\ 1 & 1 \end{bmatrix}}_{T} \begin{bmatrix} q_2 \\ q_3 \end{bmatrix} - \begin{bmatrix} 2\theta_{\mathrm{abd}}^{\mathrm{ref}} \\ 2\theta_{\mathrm{flex}}^{\mathrm{ref}} \end{bmatrix} \tag{3.25}$$

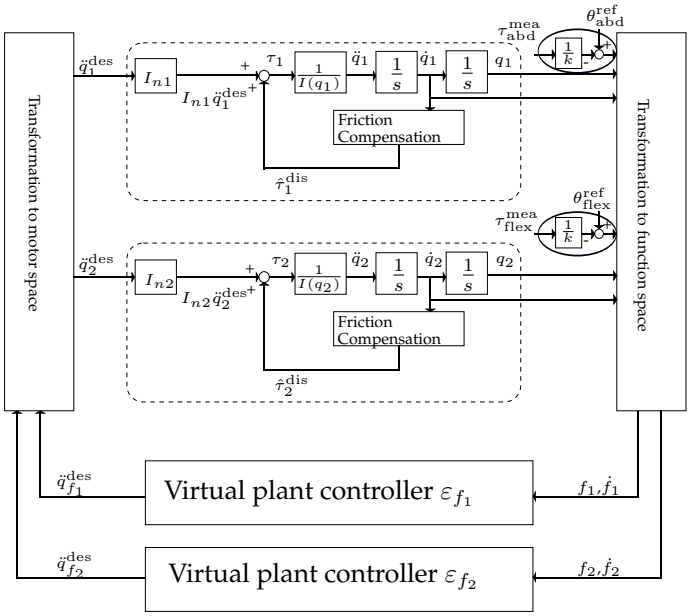

Figure 3.7: Control scheme for the base joints of the DLR/HIT Hand II

To control the obtained functions, two virtual plants are designed. In order to scale down the noise introduced by the differentiation of positions, Sabanovic and Ohnishi [2011]'s auxiliary error definition is changed. While defining the auxiliary errors ε_{f_i}, not only the functions f_i are weighted with scalars w_{i2} but also the first derivatives of the functions are weighted with scalars w_{i1} (see Equations 3.15 and 3.26). Implementing the virtual plant controllers the desired accelerations of the functions, $\ddot{q}_{f_1}^{\text{des}}$ and $\ddot{q}_{f_2}^{\text{des}}$ are obtained.

$$\begin{aligned} \varepsilon_{f_1} &= w_{11}\dot{f}_1 + w_{12}f_1, \\ \varepsilon_{f_2} &= w_{21}\dot{f}_2 + w_{22}f_2. \end{aligned} \tag{3.26}$$

The desired accelerations of the functions are transformed into the desired accelerations of motors using the inverse of T :

$$\begin{bmatrix} \ddot{q}_2 \\ \ddot{q}_3 \end{bmatrix} = T^{-1} \begin{bmatrix} \ddot{q}_{f_1}^{\text{des}} \\ \ddot{q}_{f_2}^{\text{des}} \end{bmatrix} = \frac{1}{2} \begin{bmatrix} 1 & 1 \\ -1 & 1 \end{bmatrix} \begin{bmatrix} \ddot{q}_{f_1}^{\text{des}} \\ \ddot{q}_{f_2}^{\text{des}} \end{bmatrix}. \tag{3.27}$$

In this work, instead of using disturbance observers in the torque level, friction compensation modules are used for each motor of the hand based on the results of the friction parameter estimation explained in Section 2.1.2—"Parameter Identification for a Friction Model". The disturbance observers of the virtual plant controllers deal with the unmodeled parts of friction and the other disturbances on the system . The use of disturbance observers may lead to overcompensation due to stiction [Le Tien et al., 2008]. By eliminating the disturbance observers in the torque level, the overcompensation is avoided.

Another difference of the control scheme used in this work, is the addition of compliance. The above explained controller design leads to very (infinitely [Tsuji et al., 2006]) stiff joints. To add compliance to the control scheme, an admittance approach is used and the desired functions are changed to:

$$f_1 = q_2 - q_3 - 2\left(\theta_{\text{abd}}^{\text{ref}} - \frac{\tau_{\text{abd}}^{\text{meas}}}{k_{\text{abd}}}\right) = 0, \tag{3.28}$$

$$f_2 = q_2 + q_3 - 2\left(\theta_{\text{flex}}^{\text{ref}} - \frac{\tau_{\text{flex}}^{\text{meas}}}{k_{\text{flex}}}\right) = 0, \tag{3.29}$$

where $\tau_{\text{abd}}^{\text{meas}}$ and $\tau_{\text{flex}}^{\text{meas}}$ are the measured torques along the abduction and flexion joints, and k_{abd} and k_{flex} are their stiffness values. The additional terms do not depend on the motor angles, hence the transformation matrix T is still invertible. It should be noted that low stiffness might lead to instabilities because of the noise introduced by the torque sensors. However, the achievable stiffness values are still within an acceptable range for manipulation tasks.

The designed controller's performance is compared to the performance of a PD controller which was implemented for the DLR/HIT Hand II. The results of the experiments and the comparisons are given in Section 5.3—"Comparison of a Disturbance Observer Based Functional Controller with a PD Controller".

Chapter 4

Calibration and Mapping of the Cyberglove

This chapter opens with a literature review on previous work on calibrations for the Cyberglove focusing on the work of Griffin et al. [2000] which is taken as a basis for the application of this work. The literature review is followed by Section 4.2—"Own Work", where the modifications made on the calibration procedure proposed by Griffin et al. for simultaneous calibration and mapping of the Cyberglove to the DLR/HIT Hand II are stated.

4.1 Related Work

According to Immersion Corp., the manufacturer of the Cyberglove, the relationship between the joint angles $\boldsymbol{\theta}$ of a human hand and the respective Cyberglove sensor measurements $\boldsymbol{\sigma}$, is assumed to be linear:

$$\boldsymbol{\theta} = \boldsymbol{\sigma} * \mathbf{g} + \boldsymbol{\beta}, \tag{4.1}$$

where the sensor gain $\mathbf{g}$ and the sensor offset $\boldsymbol{\beta}$ are un-

known. These values are aimed to be determined by a calibration routine. Generally, in calibration routines proposed for a dataglove users mimic several predefined hand poses. For example in Huenerfauth and Lu [n.d]'s work nineteen poses are proposed for a fine tuning (see Figures 4.1 and 4.2). The sensor values for these hand poses are recorded and fitted to Equation 4.1. For some sensors, this calibration approach cannot produce satisfactory results; especially for the sensors at the thumb [Zhou et al., 2010]. For this reason, some researchers proposed additional improvements to this intuitive approach [Griffin et al., 2000], [Hu et al., 2004], [Wang and Dai, 2009], and [Zhou et al., 2010]. Some of these proposed methods require additional hardware such as visual tracking systems [Hu et al., 2004]. For the purposes of this work, the use of additional tracking hardware is inconvenient, as the robot arms can occlude the fingers. Using a calibration with too many poses and tuning of parameters for each pose is also not desirable, as another design criteria in this work is the speed of the calibration routine. This work aims to improve the calibration and solve the mapping problem without compromising speed or requiring additional hardware.

4.1.1 Former Calibration Routine

There is an already implemented calibration routine in use for the telepresence system at DLR. According to this routine, subjects are asked to make three poses: a flat, a fist and a five pose. The flat pose (see Figure 4.1a) is used as the zero reference and the recorded sensor readings during this pose $\boldsymbol{\sigma}_{\text{flat}}$ are treated as offsets (see Equation 4.2). In order to determine gains for the flexion/extension sensors $\mathbf{g}_{\text{flex}}$, subjects are asked to make a fist (see Figure 4.1b). The fist pose is represented with predefined flexion/extension joint angles with respect to the flat pose $\boldsymbol{\theta}_{\text{fist}}$. After recording sensor values $\boldsymbol{\sigma}_{\text{fist}}$ and substituting it together with $\boldsymbol{\theta}_{\text{fist}}$ and $\boldsymbol{\beta}_{\text{flex}}$ in place of $\boldsymbol{\sigma}$, $\boldsymbol{\theta}$ and $\boldsymbol{\beta}$ to Equation 4.1, $\mathbf{g}_{\text{flex}}$ is obtained (see Equation 4.3). At the end, subjects are asked to make a five with their hands (see Figure 4.1c). This pose is also represented with predefined abduction/adduction joint angles with respect to the flat pose $\boldsymbol{\theta}_{\text{five}}$. The gains $\mathbf{g}_{\text{abd}}$ for abduction/adduction sensors are determined by performing the

(a) Flat pose

(b) Fist pose

(c) Five pose

Figure 4.1: Predefined hand poses used by the old calibration routine [Huenerfauth and Lu, n.d]

same procedure used for the flexion/extension sensor gains using the recordings for the five pose (see Equation 4.4). A major drawback of this approach is that the predefined angles for the fist pose and the five pose are not necessarily the same for all hands. Hence the accuracy of the calibration is not high. Although this calibration routine is not precise, it is still intuitive, fast, and does not require additional hardware.

$$\boldsymbol{\beta} = \boldsymbol{\sigma}_{\text{flat}}, \tag{4.2}$$

$$\mathbf{g}_{\text{flex}} = \frac{\boldsymbol{\sigma}_{\text{fist}} - \boldsymbol{\beta}_{\text{flex}}}{\boldsymbol{\theta}_{\text{fist}}}, \tag{4.3}$$

$$\mathbf{g}_{\text{abd}} = \frac{\boldsymbol{\sigma}_{\text{five}} - \boldsymbol{\beta}_{\text{abd}}}{\boldsymbol{\theta}_{\text{five}}} \tag{4.4}$$

where $\boldsymbol{\beta}$, $\mathbf{g}$, and $\boldsymbol{\theta}$ are decomposed into their flexion and abduction related parts as follows:

$$\boldsymbol{\beta} = \begin{bmatrix} \boldsymbol{\beta}_{\text{flex}} \\ \boldsymbol{\beta}_{\text{abd}} \end{bmatrix}, \mathbf{g} = \begin{bmatrix} \mathbf{g}_{\text{flex}} \\ \mathbf{g}_{\text{abd}} \end{bmatrix}, \boldsymbol{\theta} = \begin{bmatrix} \boldsymbol{\theta}_{\text{flex}} \\ \boldsymbol{\theta}_{\text{abd}} \end{bmatrix}.$$

4.1.2 An Improvement of the Former Calibration Routine

Griffin et al. [2000] used a method that does not require any additional hardware, but rather takes advantage of a kinematic chain that can be formed by a pinch pose (see Figure 4.2); there the tip of the thumb and the tip of the index finger are brought together. When the human hand is in the pinch pose, N_{hh} sets of sensor values are recorded. The variation of the unknown parameters $\Delta\mathbf{g}$ and $\Delta\boldsymbol{\beta}$ are computed using the following equation:

Figure 4.2: Pinch pose [Huenerfauth and Lu, n.d]

$$\Delta\mathbf{d} = \underbrace{\begin{bmatrix} J_1(\boldsymbol{\sigma}_1 * \mathbf{g} + \boldsymbol{\beta}) & J_1(\boldsymbol{\sigma}_1 * \mathbf{g} + \boldsymbol{\beta})diag(\boldsymbol{\sigma}) \\ \vdots & \vdots \\ J_{N_{hh}}(\boldsymbol{\sigma}_{N_{hh}} * \mathbf{g} + \boldsymbol{\beta}) & J_{N_{hh}}(\boldsymbol{\sigma}_{N_{hh}} * \mathbf{g} + \boldsymbol{\beta})diag(\boldsymbol{\sigma}) \end{bmatrix}}_{J} \underbrace{\begin{bmatrix} \Delta\boldsymbol{\beta} \\ \Delta\mathbf{g} \end{bmatrix}}_{\Delta\mathbf{p}} \quad (4.5)$$

$$\Delta\mathbf{p} = -J^{\dagger}\Delta\mathbf{d}, \quad (4.6)$$

where $\Delta\mathbf{d}$ is the vector of distances between thumb and index finger, and J_i are the jacobian matrices obtained by concatenating the jacobian matrices of the human thumb and index finger. The computed variations of the unknown parameters are used to correct sensor gain and offset. The

computation of jacobian matrices for the estimated joint angles and solving Equation 4.5 is iterated until the parameter variation or the error $\Delta\mathbf{d}$ converges. The finger segment lengths are also included in the unknown parameters in Griffin et al.'s work. The solutions obtained with this approach were not feasible. The algorithm converged to trivial solutions where either all gains are zero or all finger segment lengths are zero. In order to avoid converging to such trivial solutions, Griffin et al. limited the deviation $\boldsymbol{\rho}$ of the parameter vector $\mathbf{p}$ with respect to a predetermined "biologically feasible" parameter vector $\mathbf{p_0}$.

$$[\mathbf{p_0} - \mathbf{p}] = \mathbf{I}\Delta\mathbf{p} \tag{4.7}$$

$$V_{ii} = -\sqrt{N_{hh}}\frac{\partial}{\partial p_i}\left[\left(\frac{p_{0i} - p_i}{\rho_i}\right)^m\right], m \in \mathbb{R}_+, i \in \mathbb{N} \tag{4.8}$$

$$\begin{bmatrix} \Delta\mathbf{d}_1 \\ \vdots \\ \Delta\mathbf{d}_{N_{hh}} \\ V[\mathbf{p_0} - \mathbf{p}] \end{bmatrix} = \begin{bmatrix} \hat{J}(\boldsymbol{\sigma}_1, \mathbf{p}) \\ \vdots \\ \hat{J}(\boldsymbol{\sigma}_{N_{hh}}, \mathbf{p}) \\ V \end{bmatrix} [\Delta\mathbf{p}] \tag{4.9}$$

Equation 4.7 drives the parameter set $\mathbf{p}$ to the nominal parameter set $\mathbf{p_0}$ and the rate of convergence can be controlled by multiplying both sides of the function by a non-singular matrix V. Griffin et al. chose V as a diagonal square matrix whose elements are potential well functions for the i^{th} element of the parameter set $\mathbf{p}$ with n elements, where N_{hh} is the number of recorded poses and m is a design parameter used to adjust the potential well function (see Equation 4.8). After multiplying both sides of Equation 4.7 by V and concatenating the resulting matrices to the matrices in Equation 4.5, the deviations of the parameters is limited (see Equation 4.9). Griffin et al. also mention that, to avoid numerical instabilities due to p_i getting too far away from the variances, the step size of the optimization iteration is reduced adaptively. However, the adaptive scaling of the step size is not explained in their paper.

In this work, Griffin et al.'s idea is adapted for achieving the calibration of the Cyberglove and the mapping between the Cyberglove and the DLR/HIT Hand II. This is explained in the next section.

4.2 Own Work

It is hypothesized that while using the telepresence system, the human operator would tend to use his/her hands similar to the robot hands, so that he/she would be able find configurations of the robot hand that can achieve the desired task more easily. Also, the handles of the HMI contributes to this hypothesis by applying constraints on the palm movements of the human operator. By this token, Griffin et al.'s work is tailored for the needs of this work as follows; the finger segment lengths are excluded from the estimation parameters, and the jacobian matrices for DLR/HIT Hand II are used instead of human hand jacobian matrices. By doing so, the sensor outputs of the dataglove are aimed to be mapped directly to the robotic hand instead of trying to find the actual human hand pose, and then mapping this pose to the robotic hand's workspace.

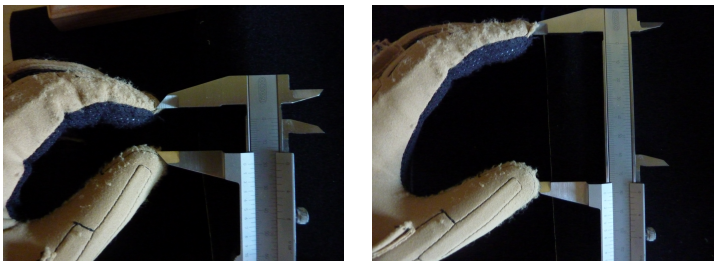

(a) 2 cmopening **(b)** 8 cmopening

Figure 4.3: Example hand poses used by the new calibration routine

Using the former calibration routine, the actual pose of the human hand is already known up to some extent and it is mapped to the robotic hand workspace with a direct joint space mapping. Then, Griffin et al.'s idea is used for a Cartesian space correction of the robotic hand's pose, i.e. the offsets and gains are optimized for the desired finger tip distances. In order to have more information about the relation between the human hand and the robotic hand workspaces, the sensor outputs are recorded not only during pinch pose, but also when there is a gap between the tip of the thumb and the tip of the index finger (see Figure 4.2). The distance between the tip of the thumb and index finger is increased with 1 cmincrements using a caliper,

and the corresponding sensor values are recorded. It is assumed that during these hand poses abduction angle of the index finger is zero. This assumption leads to the following form of the jacobian matrices $J_i \in \mathbb{R}^{3\times5}$:

$$J_i = \left[\begin{array}{cc} J_{\text{thumb}} & J_{\text{index}} \end{array} \right], \tag{4.10}$$

where $J_{\text{thumb}} \in \mathbb{R}^{3\times3}$ is the jacobian matrix for a finger module of the DLR/HIT Hand II and $J_{\text{index}} \in \mathbb{R}^{3\times3}$ is the same jacobian matrix excluding the column that is related to the abduction joint. These jacobian matrices J_i are used to construct the J matrix in Equation 4.5.

Also, the desired distances between the finger tips are subtracted from the distances computed by the forward kinematics of the robotic hand using the joint angle measurements. The resulting vector replaced $\Delta\mathbf{d}$, which appears on the left side of Equation 4.5. The iterative sensor gain and offset value computation method, which is explained in Section 4.1.2—"An Improvement of the Former Calibration Routine", is applied to this data.

The Cyberglove calibration and mapping routine explained above was tested and two problems were observed. These problems are namely:

- instabilities: sometimes the optimization routine does not converge, but instead starts oscillating,
- infeasible solutions: some solutions tend to generate parameters sets which would result in motions outside the workspace of the robotic hand, i.e. saturating solutions.

4.2.1 Instability

In order to overcome the instability problem, the parameter correction vector $\Delta\mathbf{p}$ and its step size is changed adaptively using Fletcher-Reeves conjugate gradient algorithm

[Fletcher and Reeves, 1964]. Previously, $\Delta\mathbf{p}$ was given by the Equations 4.5 and 4.6.

With Fletcher-Reeves conjugate gradient algorithm the parameter correction vector $\Delta\mathbf{p}$ is modified as follows:

$$\begin{array}{ll} \Delta\mathbf{p}^{(1)} = -(J^{(0)})^{\dagger}\Delta\mathbf{d}^{(0)} & k = 1 \\ \Delta\mathbf{p}^{(k)} = -(J^{(k-1)})^{\dagger}\Delta\mathbf{d}^{(k-1)} + \gamma\Delta\mathbf{p}^{(k-1)} & k > 1 \end{array} \tag{4.11}$$

where γ is given by

$$\gamma = \frac{\|(J^{(k-1)})^{\dagger}\Delta\mathbf{d}^{(k-1)}\|_2^2}{\|(J^{(k-2)})^{\dagger}\Delta\mathbf{d}^{(k-2)}\|_2^2} \tag{4.12}$$

and k is the number of iterations. Then, the length of the parameter correction vector $\Delta\mathbf{p}$ is scaled by α such that the error objective is minimized (see Equation 4.13). This line search is performed using the *fminsearch* function of MATLAB.

$$\begin{bmatrix} \boldsymbol{\beta} \\ \mathbf{g} \end{bmatrix}^{(k)} = \begin{bmatrix} \boldsymbol{\beta} \\ \mathbf{g} \end{bmatrix}^{(k-1)} + \alpha\Delta\mathbf{p}^{(k)} \tag{4.13}$$

4.2.2 Infeasible Solutions

Like Griffin et al.'s work, the problem of infeasible solutions was solved by limiting the parameters around a previously determined good parameter set $\mathbf{p}_0$. For limiting the elements of a parameter set $\mathbf{p}$, potential well functions V_{ii} used in Griffin et al. are also used in this work (see Equation 4.8). The variations of the parameters with respect to the nominal parameter set is limited and feasibility of the resulting parameter set are ensured by using these functions in the optimization routine(see Section 4.1.2).

Chapter 5

Experimental Evaluation

In this chapter experimental evaluation results of the friction compensation and the functional controller are presented for the base joint of the thumb of DLR/HIT Hand II. The thumb is chosen because it has more operational space which is not occluded by the other fingers. Another reason for using the thumb is the dramatic disturbance torque difference of the base joint motors of the finger module which is currently mounted as the thumb. Following the previous indexing convention for the DLR/HIT Hand II, the motors at the base joint are called the 2^{nd} and 3^{rd} motor in the rest of the chapter (see Section 1.3—"Slave Side: DLR/HIT Hand II").

5.1 Experimental Setup

The experiments are performed with a left-handed DLR/HIT Hand II (see Section 1.3—"Slave Side: DLR/HIT Hand II"), and a left-handed Cyberglove (see Section 1.4—"Master Side: Dataglove"). The DLR/HIT Hand II is connected to a real-time computer running VxWorks[1], a real-time operating system, whereas the Cyberglove is connected to a PC running Linux via Bluetooth. The sensory data of the Cyberglove is sent to the real-time

[1]http://www.windriver.com/products/vxworks/, Date accessed: 24 August 2011

computer using UDP. The control model is built using Matlab/Simulink Real-Time Workshop, and the External Mode[2] option of Simulink is used for connecting to the VxWorks target.

5.2 Friction Compensation

Using the Matlab GUI, which is described in Section 2.2.2—"A Graphical User Interface for the Identification of the Friction Parameters", friction parameters of the motors of the thumb of the DLR/HIT Hand II are estimated in eight consecutive runs of the calibration routine. According to the calibration routine, all three motors of a finger module are commanded to move at four different constant velocity levels and during the movement, the commanded torques are recorded. The method used by Connette [2006] and the method introduced in this work are used to estimate the friction parameters in question. The two methods are compared in terms of condition numbers and torque estimation errors. The new method resulted in smaller sum of squared errors (see Figures 5.1 and 5.2).

In all runs the identified parameters resulted in physically feasible friction models, i.e. all identified parameters are non-negative and all of the resulting friction models are consistent to one another. The maximum and the minimum friction torque estimations of all runs are depicted in Figures 5.3 and 5.4. The maximum difference between the maximum and minimum estimated torques is less than 0.06 $\mathrm{Nm}$for velocities less than 2 $\mathrm{rad/s}$(see Figures 5.5 and 5.6).

Also, the resulting models are good at estimating the commanded torques while the motors are moving at a constant velocity, especially in the positive direction. Whereas the torque estimation could not reflect the torque overshoots at the instances when the direction of motion is changed (see Figures 5.7 and 5.8).

The outputs of the friction compensation module are also

[2] http://www.mathworks.de/help/toolbox/rtw/ug/f996923.html, Date accessed: 24 August 2011

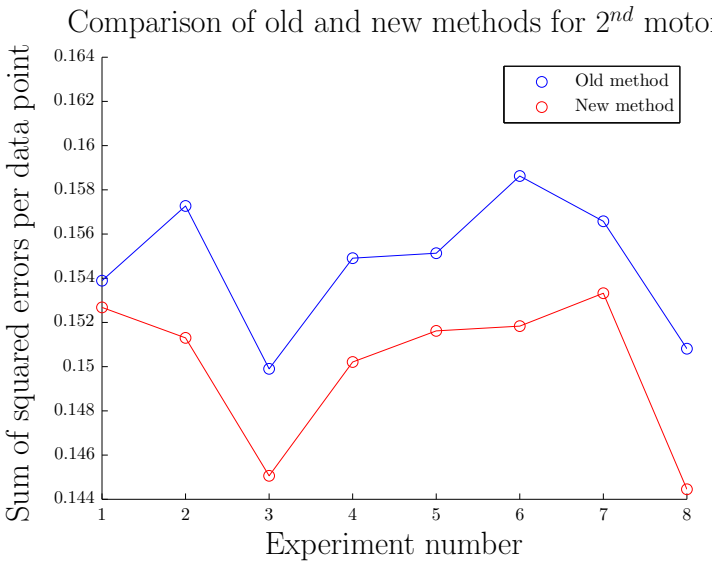

Figure 5.1: Comparison of estimation errors for the 2^{nd} motor of the thumb in eight runs of the calibration routine

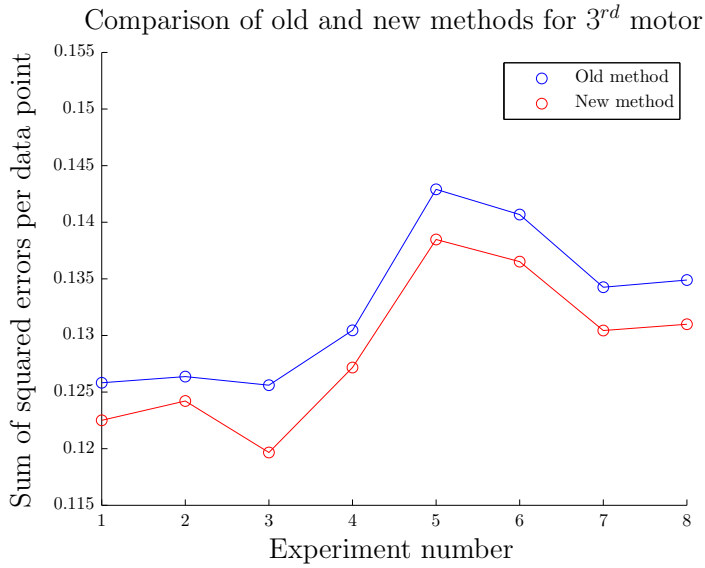

Figure 5.2: Comparison of estimation errors for the 3^{rd} motor of the thumb in eight runs of the calibration routine

compared with the outputs of a torque level disturbance observer. The comparisons are performed under three cases; external torque, step position reference, and blended trajectory reference (trapezoidal velocity profile) (see Fig-

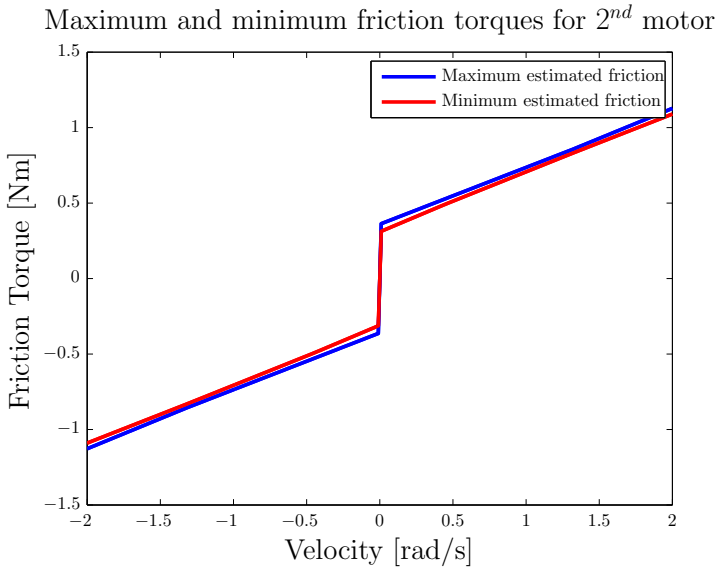

Figure 5.3: Maximum and minimum estimated friction for the 2^{nd} motor of the thumb in eight runs of the calibration routine

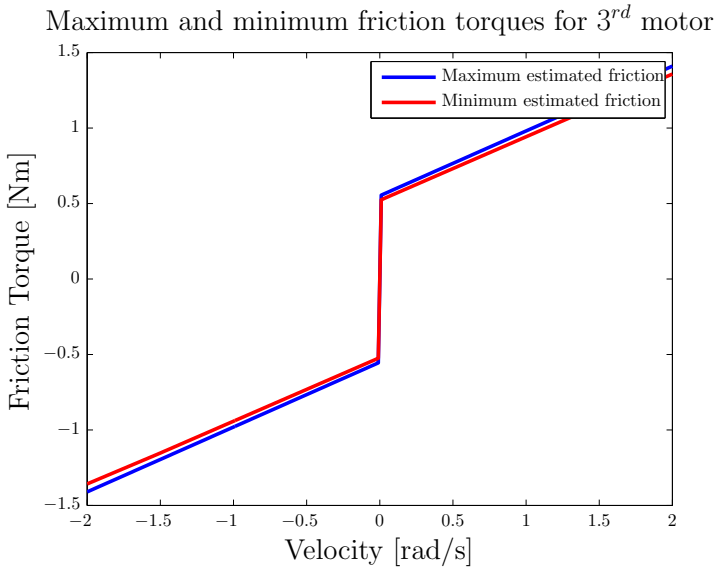

Figure 5.4: Maximum and minimum estimated friction for the 3^{rd} motor of the thumb in eight runs of the calibration routine

ure 5.9). Although the output of the torque level disturbance observer is not necessarily the actual disturbance

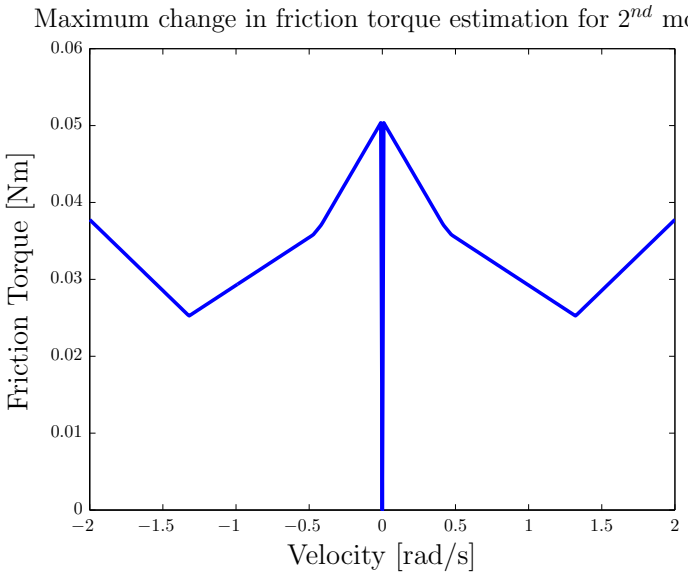

Figure 5.5: Difference of maximum and minimum estimated friction torques for the 2^{nd} motor of the thumb in eight runs of the calibration routine

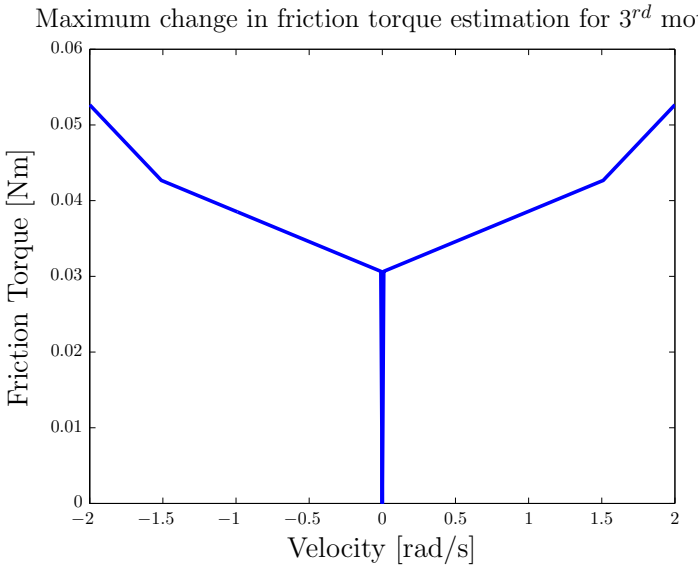

Figure 5.6: Difference of maximum and minimum estimated friction torques for the 3^{rd} motor of the thumb in eight runs of the calibration routine

torque, it can still be used as a means of evaluating the quality of the friction compensation. The external torque

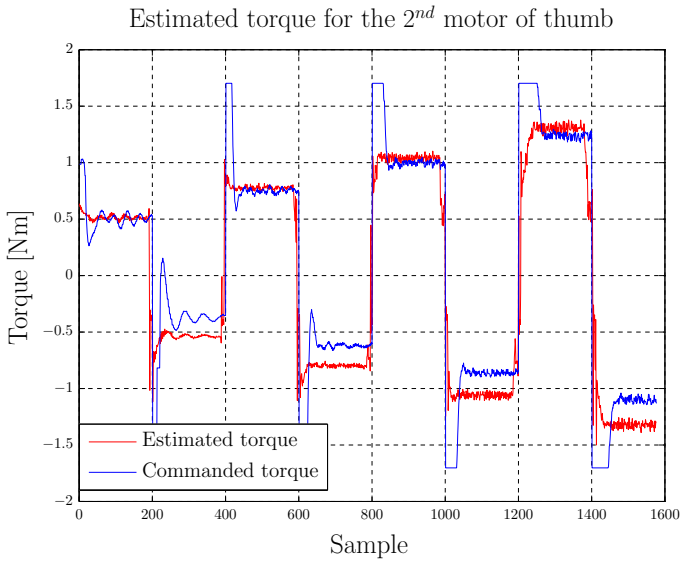

Figure 5.7: Commanded torque vs estimated torque for the 2^{nd} motor of the thumb for the last one of the calibration runs

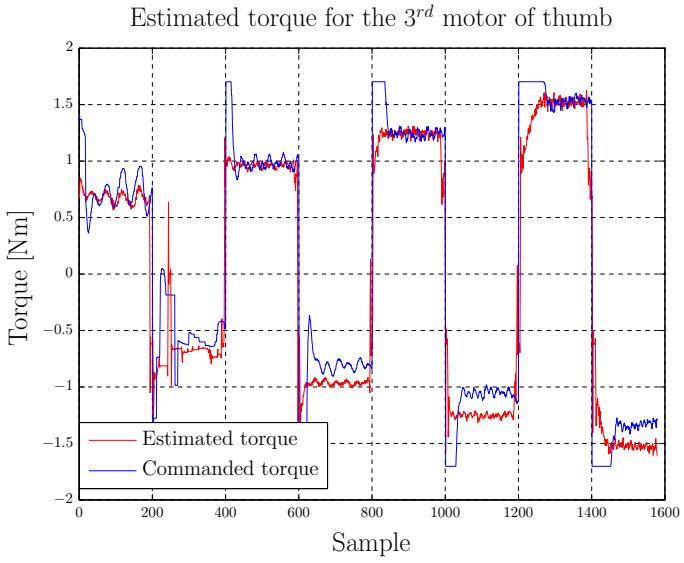

Figure 5.8: Commanded torque vs estimated torque for the 3^{rd} motor of the thumb for the last one of the calibration runs

case is chosen for comparisons in the presence of disturbance torques other than the friction. On the other hand,

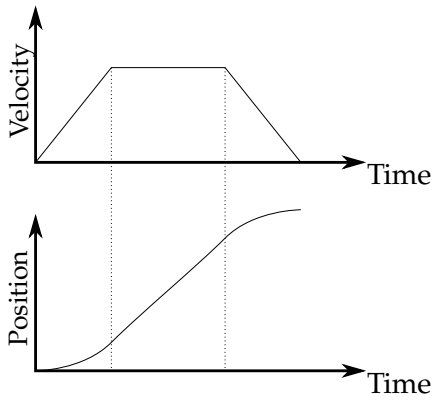

Figure 5.9: Blended trajectory profile

the step position reference and the blended trajectory reference are chosen for comparisons under different accelerations which would influence the actual friction behavior.

The control scheme used during the comparison is different from the one introduced in Section 3—"Controller Design". In this case, the output of the torque level disturbance observer is fed back and the output of the friction compensation module is not added to the measured torques. In external torque case, the finger is commanded to stay at its initial position and it is moved back and forth by hand. In the step position reference and blended trajectory reference cases, the position reference is changed with a ten degrees step input and a ten degrees displacement according to the position profile depicted in Figure 5.9, respectively.

For the external torque case, the magnitudes of the disturbance observer outputs and the friction compensation module outputs are close to each other (see Figures 5.10 and 5.11), whereas for the step position reference case, the disturbance observer's output is significantly larger than the friction compensation module's (see Figures 5.12, and 5.13). Contrary to the first two cases, friction compensation module generated higher torque outputs compared to the outputs of the disturbance observer for the blended trajectory reference case (see Figures 5.14, and 5.15).

These results agree with the the exclusion of the torque

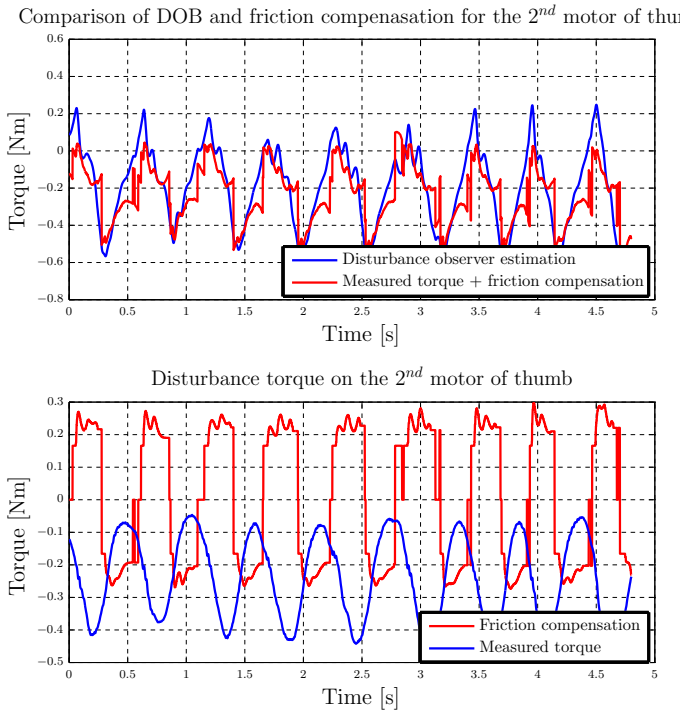

Figure 5.10: Comparison of DOB estimation and friction model estimation for the 2^{nd} motor of the thumb with external torque

level disturbance observer and validates the use of the friction compensation. For the external torque case getting similar magnitudes for the compensation torques can be interpreted as good quality of the friction estimation. On the other hand, the dramatic difference between the magnitudes in the step position reference case is possibly due to the stiction overcompensation of the disturbance observer [Le Tien et al., 2008], which is undesirable as adding extra energy to the system might lead to instability. The last case is expected to be a challenging situation for the friction compensation because the break-up torque to overcome stiction gets higher if the commanded torque is increased slowly [Olsson et al., 1998]. The chosen friction model does not take this into consideration, so the higher torques generated by the friction compensation is desirable for overcoming the stiction. One should also keep in mind that the reference position is changed slowly, compared to

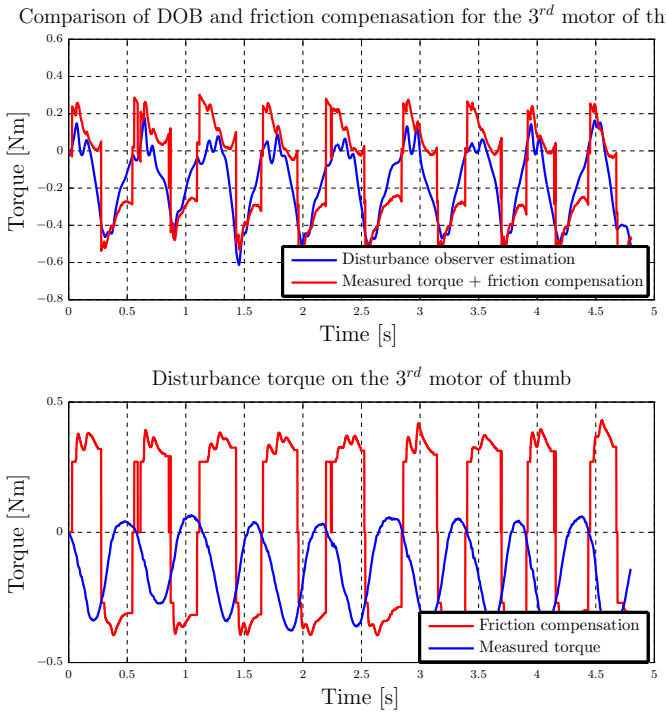

Figure 5.11: Comparison of DOB estimation and friction model estimation for the 3^{rd} motor of the thumb with external torque

the step reference, and additionally, the friction compensation module helped the overcoming the friction, so it is reasonable for the disturbance observer to generate lower torques. When the friction compensation module is turned off, the output of the disturbance observer becomes higher than the torque estimated by the friction model (see Figures 5.16, and 5.17).

The performance of the friction compensation is further investigated in the following section. The performances of a PD controller and a functional controller are compared under cases of friction compensation and no friction compensation.

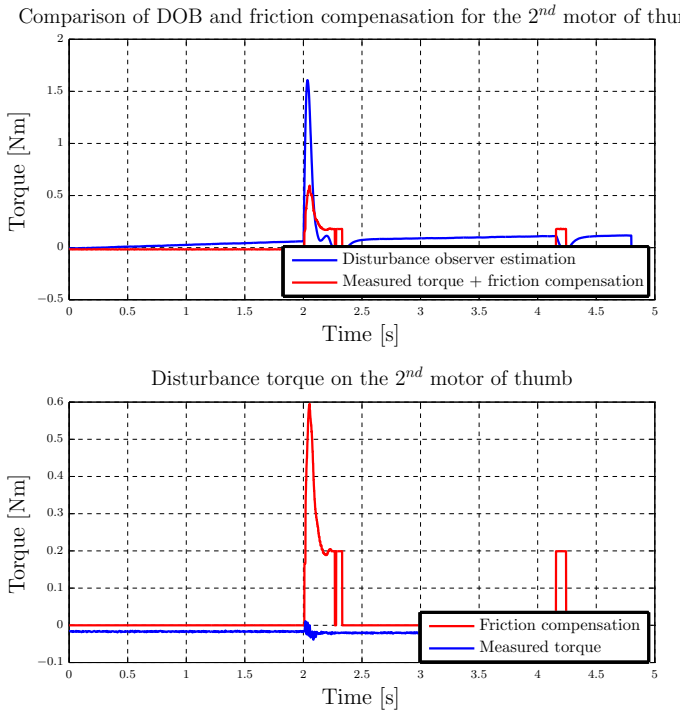

Figure 5.12: Comparison of DOB estimation and friction model estimation for the 2^{nd} motor of the thumb with step position reference

5.3 Comparison of a Disturbance Observer Based Functional Controller with a PD Controller

Step responses and reference tracking performances of the disturbance observer based functional controller and conventional PD controller are compared to each other along different movement directions (see Figure 5.18), for two cases: with friction compensation module turned on or off. The movement directions are chosen such that the controllers can be compared for different synchronization relations of the two motors at the base joint. These directions are depicted in Figure 5.18 where the arrows indicate vectors along which the movement is performed, e.g. flexion/extension, and the letters in parentheses indicate the corresponding figures for the movement directions,

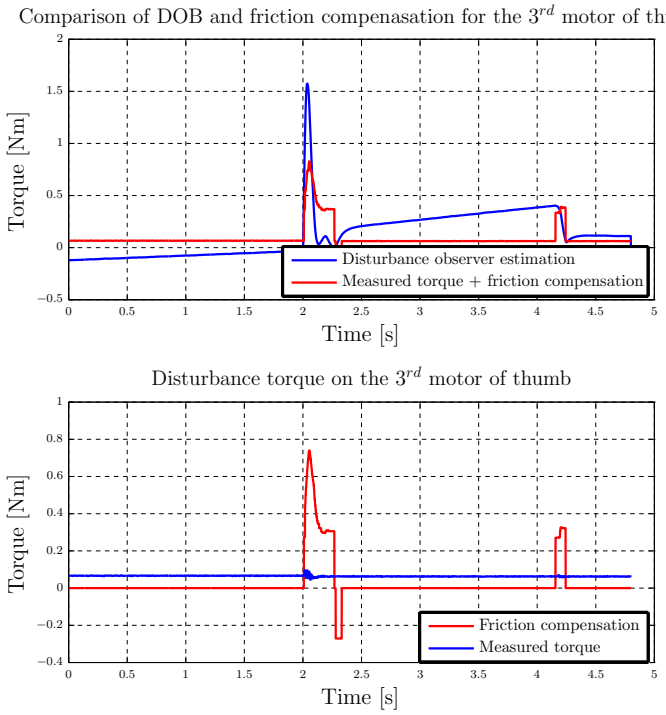

Figure 5.13: Comparison of DOB estimation and friction model estimation for the 3^{rd} motor of the thumb with step position reference

e.g. (a) denoting the flexion and (b) denoting the extension. The letters in parentheses also correspond to the subfigures, e.g. position results for the pure flexion commands are depicted in Figure 5.19a.

The commanded step references five degrees step changes in the given movement direction, and the reference tracking references are blended trajectories (see Figure 5.9) of five degrees position change.

For the step references along the flexion/extension direction, i.e. equal motor angle references, the function based controller outperformed the PD controller both in terms of step response and the deviation along the abduction/adduction direction (see Figures 5.19a and 5.19b). Note that the deviation in the case of a PD controller without friction compensation is also small, but the flexion

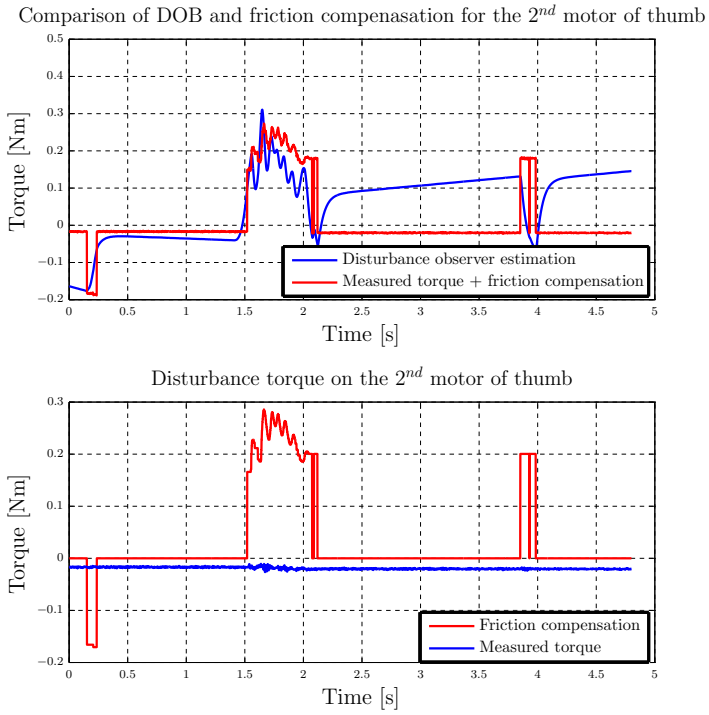

Figure 5.14: Comparison of DOB estimation and friction model estimation for the 2^{nd} motor of the thumb with blended trajectory reference

movement is very small, so this small deviation is not an outcome of the good controller performance. Also, for the different controllers, the friction compensation resulted in different behavior. For the functional controller, the friction compensation resulted in smoother trajectories, better transients and smaller deviation for flexion command, but not a better steady-state error. On the other hand, for a PD controller it resulted in smaller errors, but dramatically more deviation. The abduction/adduction deviation is almost as large as the flexion/extension movement. This means that the 3^{rd} motor almost does not move. One can also observe the different performances of the PD controller for the reference along the 2^{nd} motor and along the 3^{rd} motor (see Figures 5.19f, 5.19e, 5.19h and 5.19g). However, the difference between the performance for movements along different motors is not so dramatic as in the case of references along the flexion/extension direction. The dramatic differ-

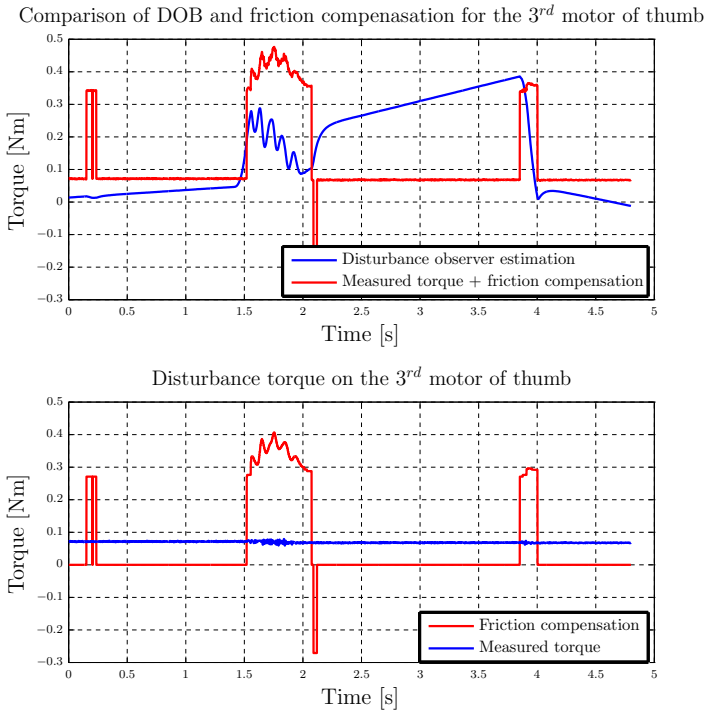

Figure 5.15: Comparison of DOB estimation and friction model estimation for the 3^{rd} motor of the thumb with blended trajectory reference

ence is possibly a result of the mechanical coupling of the motors.

When step references are commanded along the abduction/adduction direction, i.e. equal motor angle references with different signs, the above discussion is still valid (see Figures 5.19c and 5.19d). On the other hand, when the commanded references are along the directions of single motors, the behavior of the functional controller both with or without friction compensation is very similar to one another. Nevertheless, presence (or absence) of the friction compensation affects the behavior of the PD controller significantly. The PD controller with friction compensation performed as good as the functional controller for the case of commands along the 2^{nd} motor. Although the performance of the PD controller with friction compensation improved also for the commands along the 3^{rd} motor, it is still

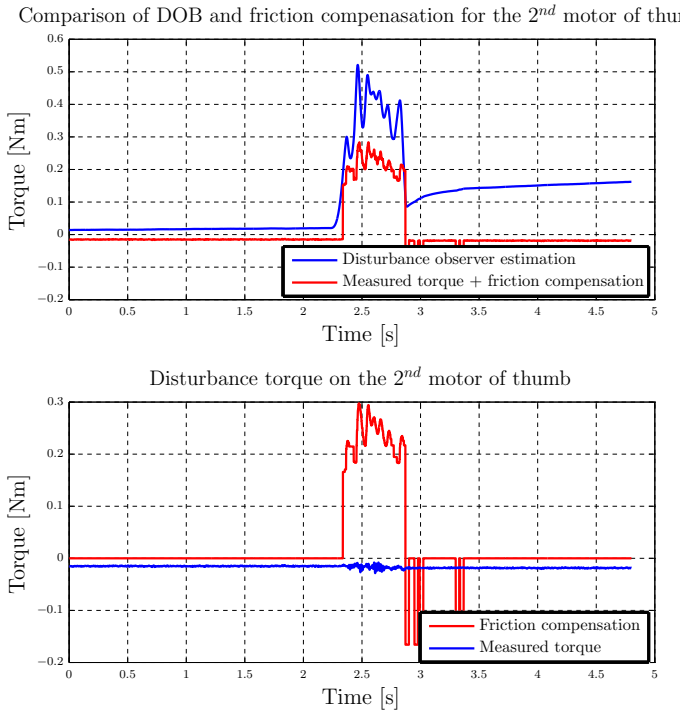

Figure 5.16: Comparison of DOB estimation and friction model estimation for the 2^{nd} motor of the thumb with blended trajectory reference

not as good as the performance of the functional controller. Performances of both controllers with or without friction compensation are better for commands along the 2^{nd} motor compared to the performances for commands along the 3^{rd} motor (see Figures 5.19f, 5.19e, 5.19h and 5.19g).

The main properties of the controllers discovered at step responses also apply to the blended trajectory tracking (see Figure B.1 in Appendix B—"Controller Evaluation for Blended Reference").

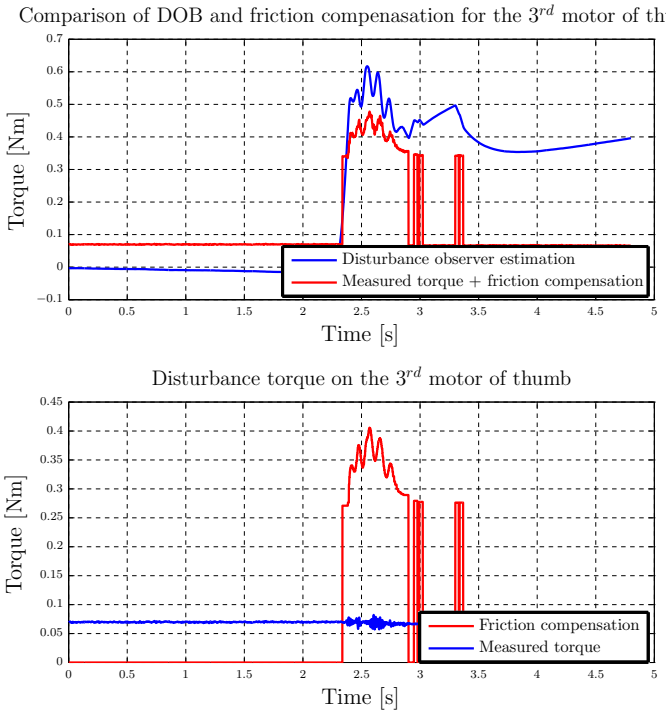

Figure 5.17: Comparison of DOB estimation and friction model estimation for the 3^{rd} motor of the thumb with blended trajectory reference

5.4 Calibration and Mapping of the Cyberglove

The routine which is explained in Section 4—"Calibration and Mapping of the Cyberglove", is implemented in Matlab and incorporated into the Matlab GUI explained in 2.2.2—"A Graphical User Interface for the Identification of the Friction Parameters". In order to evaluate the performance, subjective opinions of users who have previously used the HMI, are taken into account. These subjective opinions are used as the only evaluation criterion because the ground truth, the actual human hand pose, is not known.

Three people who had previously used the Human Machine Interface (HMI) tried the new Cyberglove calibration

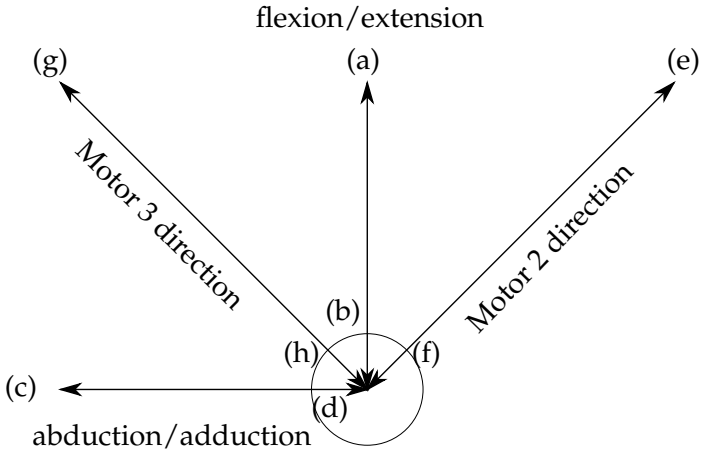

Figure 5.18: Movement directions for the comparison - letters in parentheses indicate the corresponding figures for the movement directions, e.g. position results for the pure flexion commands are depicted in the subfigure (a) of the corresponding figure

and mapping while the robotic hand was fixed on the table. All three agreed that after the new calibration and mapping, controlling the robot hand is intuitive and possibly better than their previous experience, but they also added that in order to have a better opinion, they need to use the whole setup, i.e. doing manipulation by controlling Justin via the HMI. Because the setup was not ready at the time, this was not possible.

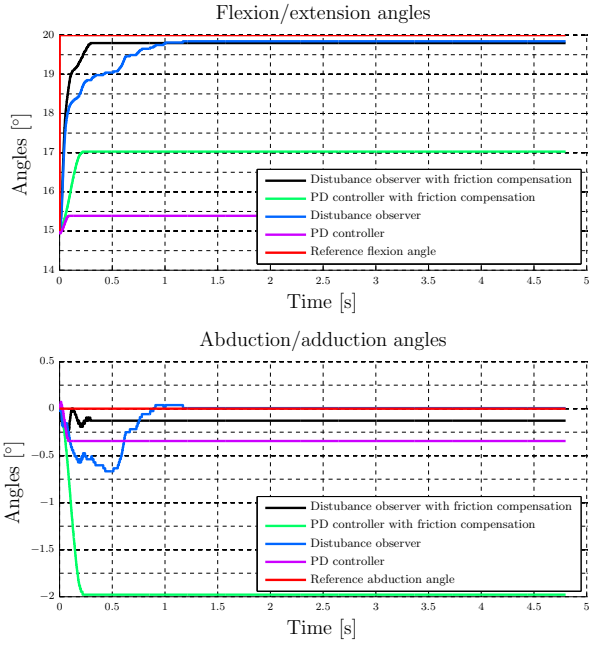

(a) Only flexion command

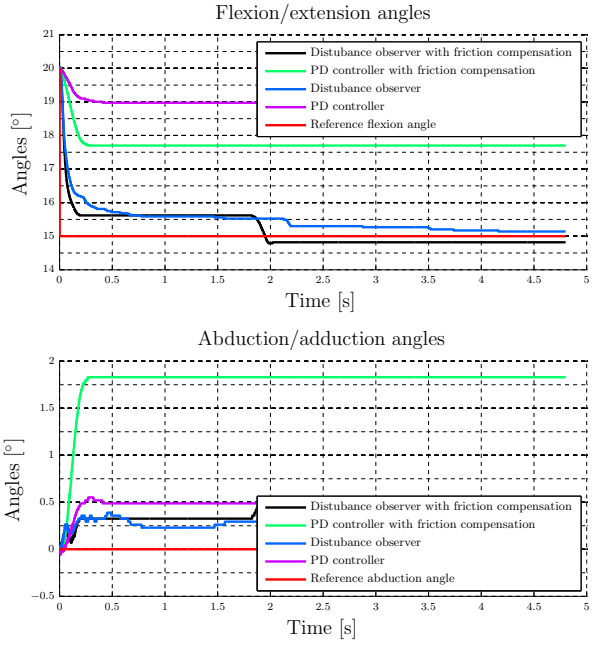

(b) Only extension command

Figure 5.19

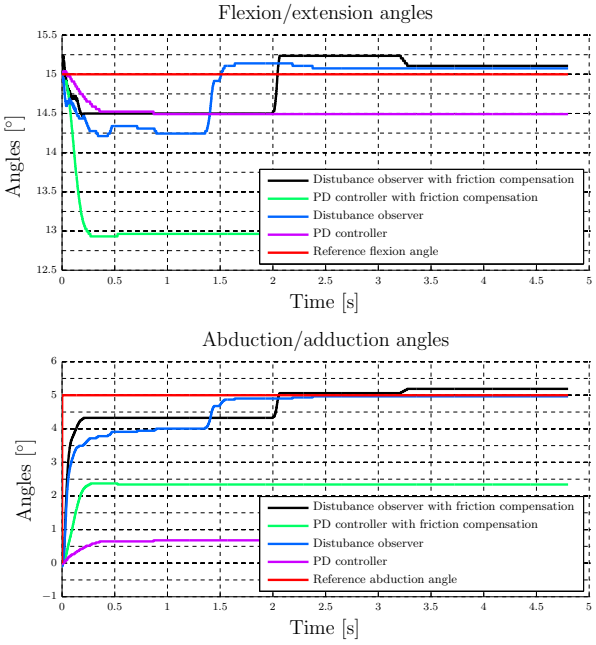

(c) Only abduction command

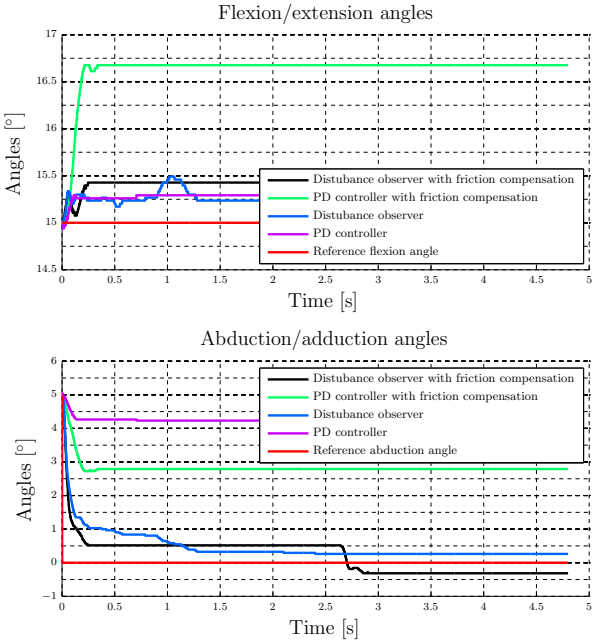

(d) Only adduction command

Figure 5.19

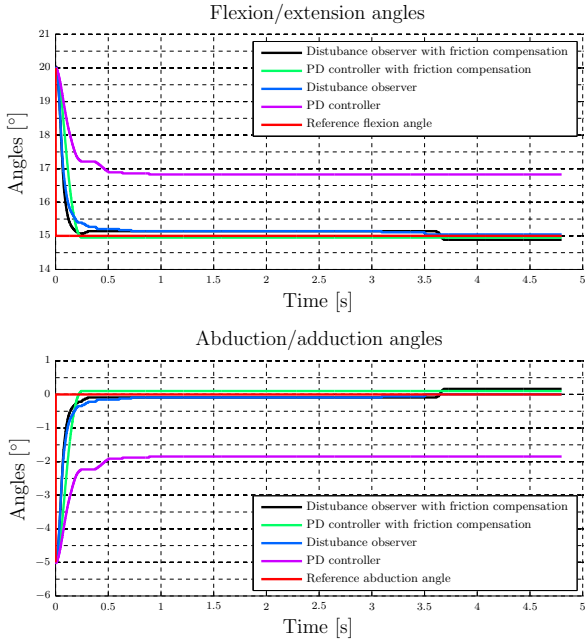

(e) Flexion and abduction along the 2^{nd} motor

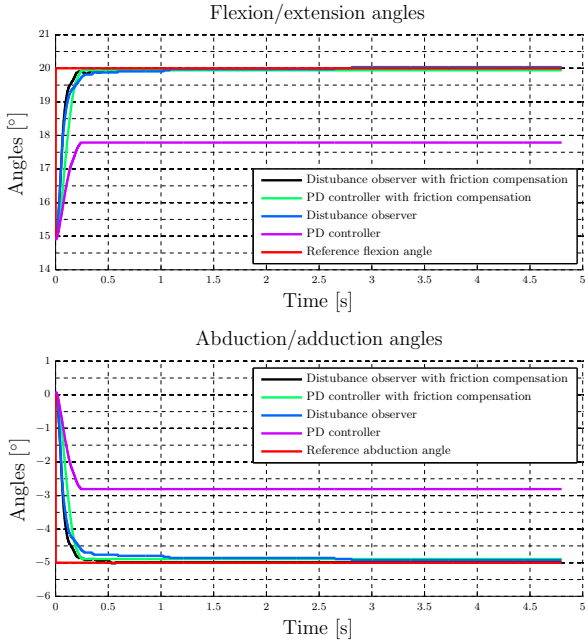

(f) Extension and adduction along the 2^{nd} motor

Figure 5.19

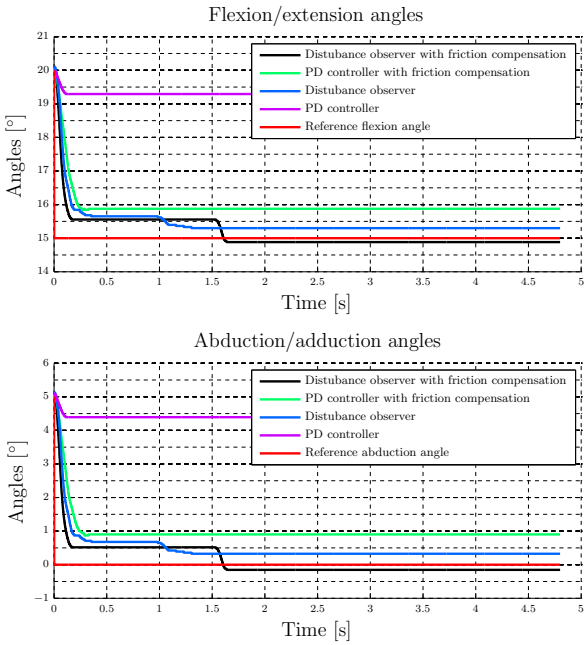

(g) Flexion and abduction along the 3^{rd} motor

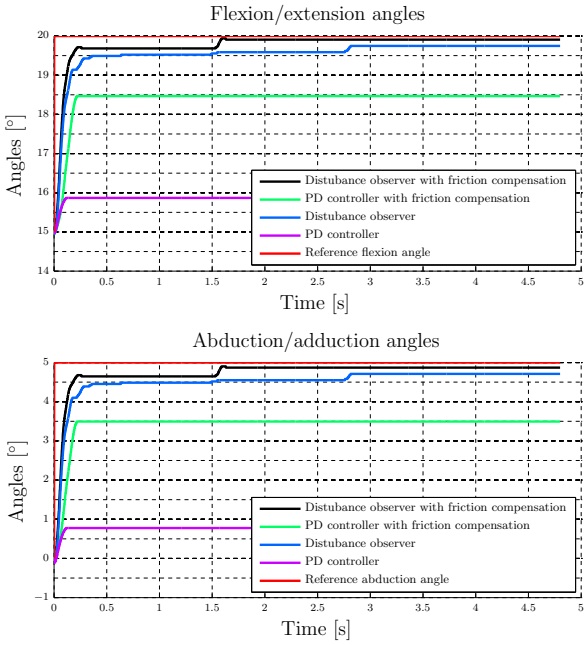

(h) Extension and adduction along the 3^{rd} motor

Figure 5.19: Step reference - responses of the DOB based controller (with and without friction compensation) and the PD controller (with and without friction compensation)

Chapter 6

Summary and Future Work

6.1 Summary and contributions

In this work, the user immersion experience in a telepresence system is be enhanced with focus on manipulation tasks. Because of the crucial role of the hands in manipulation tasks, closing the gap between a human user's hand movements and the movements of a remotely controlled robot hand would directly affect the immersion experience. To close this gap two main goals are set: the interpretation of the user intentions by a proper mapping between the human hand and the robot hand, within the limits of the robotic hands capability, to realize the intended movements, and improvement of the accuracy of the robot hand's ability to track position references.

For the interpretation of the user intentions, first the human hand movements are measured by a dataglove, namely the Cyberglove. Its sensors need a sensitive calibration for accurate measurement of the human hand movements. Furthermore, the measured hand movements need to be mapped to the robotic hand's workspace. Both of these challenges are solved by a single routine. The implemented routine is fast and does not require any additional hardware other than a caliper. By taking advantage of the an-

thropomorphic design of the hand, this method fuses the joint (configuration) space mapping and Cartesian space mapping (finger tip mapping) unlike other methods which use either one of the mapping methods (see Section 4—"Calibration and Mapping of the Cyberglove").

In order to realize the intended movements, the robotic hand used in this study is the DLR/HIT Hand II. The fingers of the DLR/HIT Hand II have high friction due to the transmission components used at the base joints, and in order to be able to track the given joint space references, the two motors at base joint have to be moved synchronously because of their mechanical coupling. By designing a controller based on the functionally related systems framework, these two control challenges are solved (see Section 3—"Controller Design"). For the compensation of friction, a friction compensation module is integrated to the control scheme. Although this control scheme can still fulfill the functional goals in the presence of high friction, the performance is improved with the addition of a friction compensation module. In order to estimate the friction parameters to be used by the friction compensation module, a parameter identification routine is implemented with a generic graphical user interface which is not exclusive to the DLR/HIT Hand II (see Section 2—"Friction Compensation").

6.2 Future work

Although the results show improvement for all the tasks that are handled in this work, there is still room for improvement. To begin with, the model used for the friction compensation does not cover all aspects of the actual friction behavior. Ways of using more complicated friction models can be investigated. But still, it should be kept in mind that this is a very challenging task and it is not guaranteed to achieve tangible improvement as the functional controller can already inherently deal with friction.

The functional controller used in this work is robust and it is able to synchronize the two motors mounted at the

metacarpophalangeal joint of the robotic fingers, but the admittance controller that is incorporated into the control scheme, does not allow low stiffness values because of torque measurement noise. Other ways of achieving compliance, which would not limit the range of achievable stiffness values, can be looked for.

The lack of a comprehensive evaluation of the dataglove calibration and mapping routine should also be addressed in a future work. Though operating the robotic hand with a dataglove using the resulting mapping is described as intuitive by three people who have previously used the HMI, a better evaluation of the results would be more conclusive. Opinions of more people can be taken into account, and some additional hardware, for example optical trackers, can be used to verify the results.

Appendix A

A Matlab GUI for Friction Parameter Identification

The Matlab GUI implemented for the identification of the friction parameters is explained in Section 2.2.2—"A Graphical User Interface for the Identification of the Friction Parameters". Once the parameter identification is started, the GUI guides the user through the necessary steps. The part of the guide that provides this guidance is shown in the following figures.

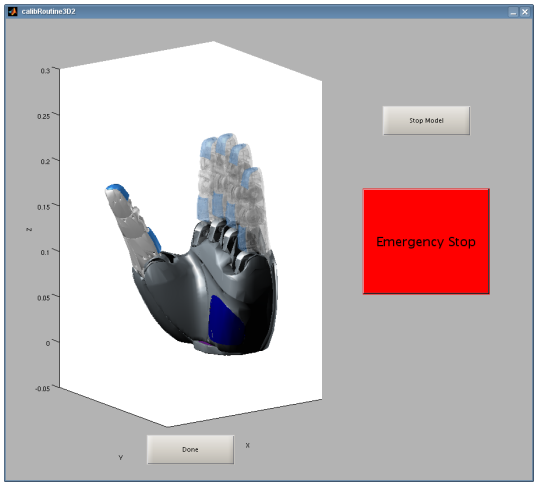

Figure A.1: Low motor limit for 1^{st} motor

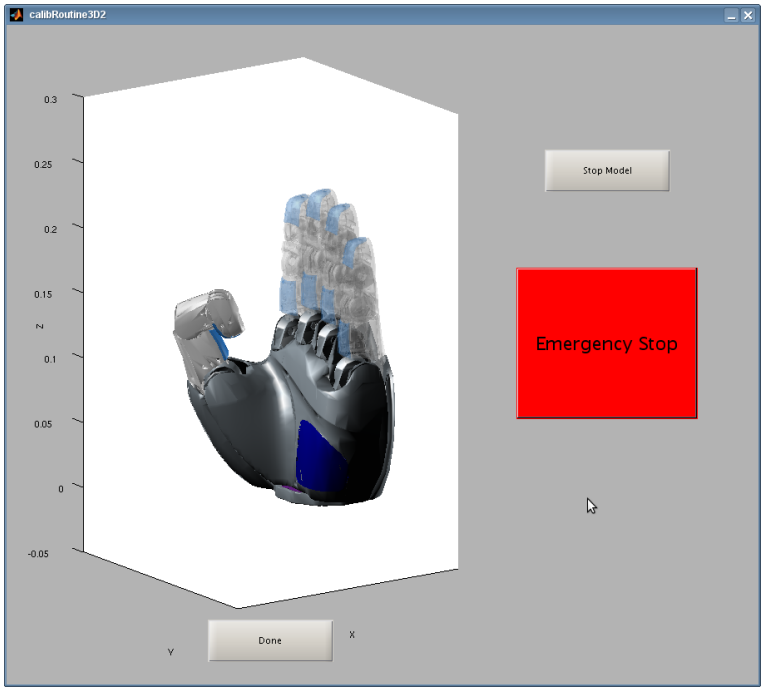

Figure A.2: High motor limit for 1^{st} motor

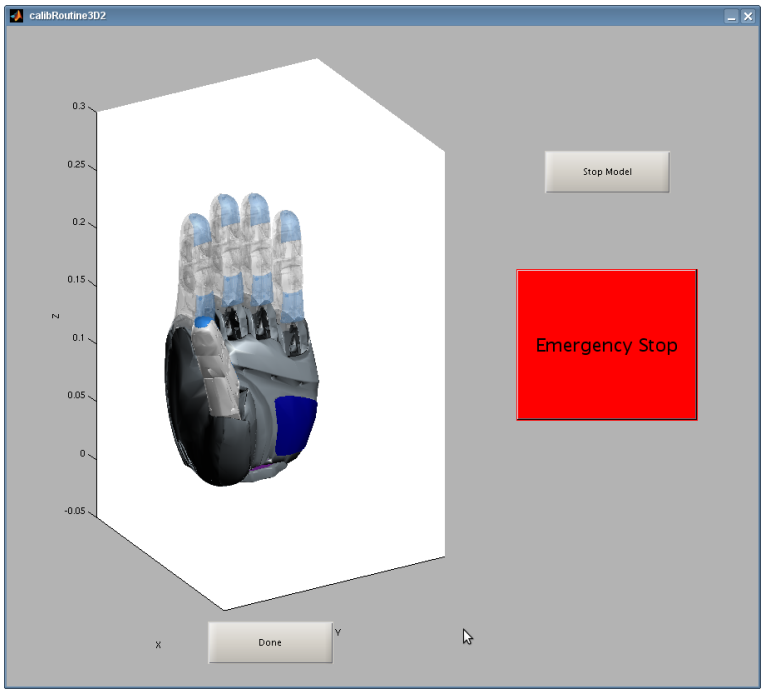

Figure A.3: Low motor limit for 2^{nd} motor

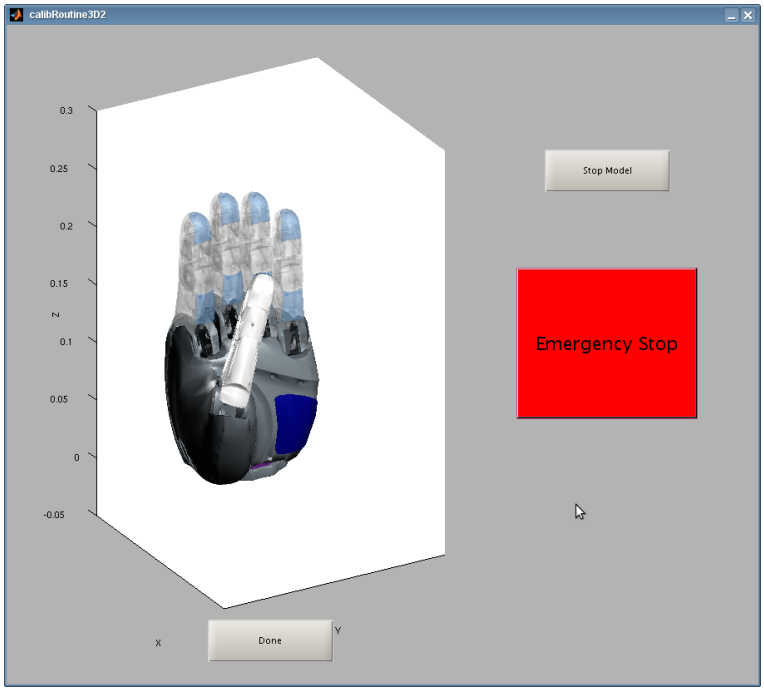

Figure A.4: High motor limit for 2^{nd} motor

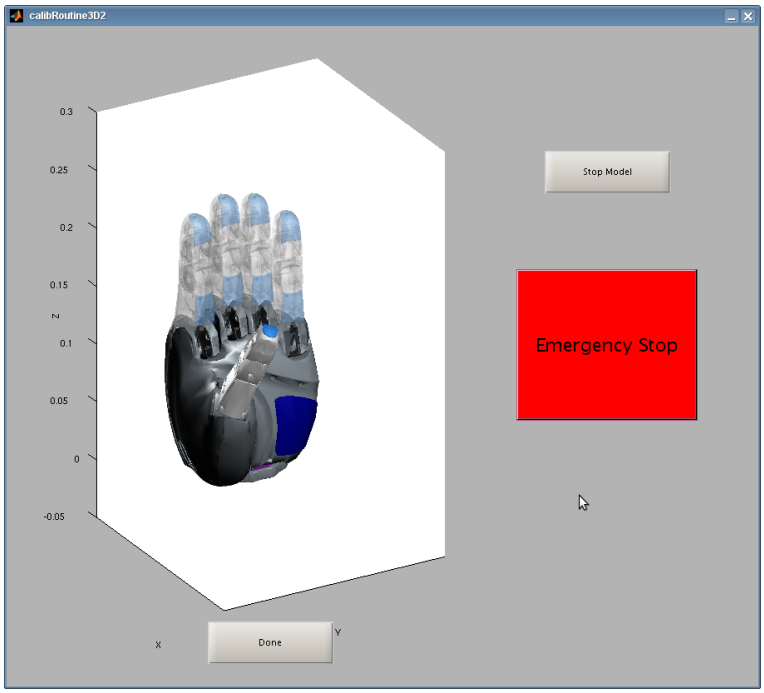

Figure A.5: Low motor limit for 3^{rd} motor

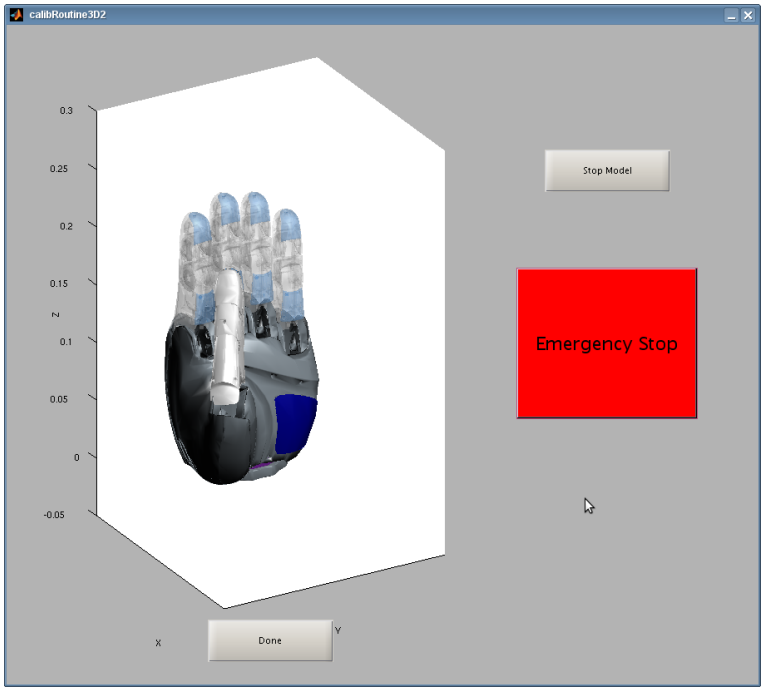

Figure A.6: High motor limit for 3^{rd} motor

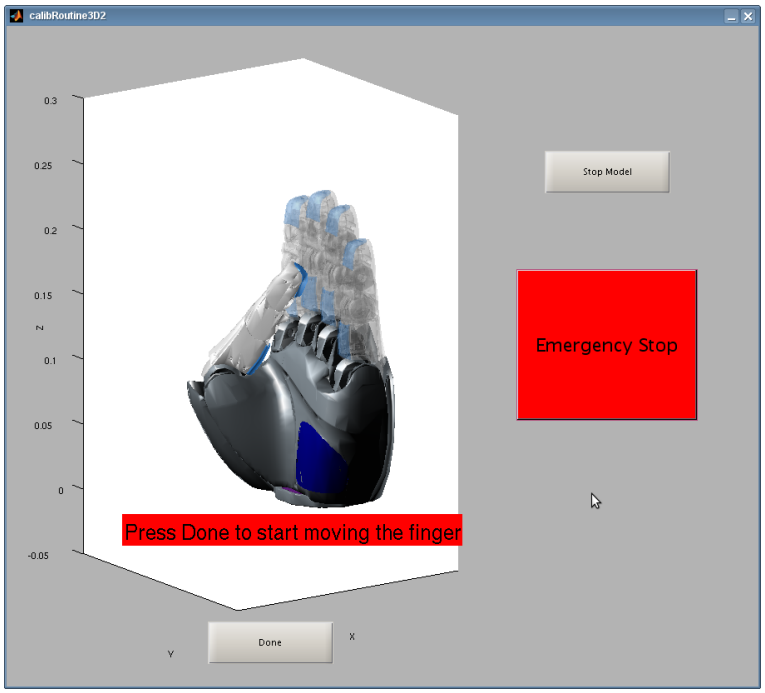

Figure A.7: Wait for start command

Appendix B

Controller Evaluation for Blended Reference

In Section 5.3—"Comparison of a Disturbance Observer Based Functional Controller with a PD Controller", the controller designed in this work is compared to the previously implemented PD controller with and without friction compensation for step position references. In this section, the results of the same comparisons are given for the blended trajectory references. The movement directions are depicted in Figure 5.18.

The main properties of the controllers discovered at step responses also apply to the blended trajectory tracking (see Figure B.1).

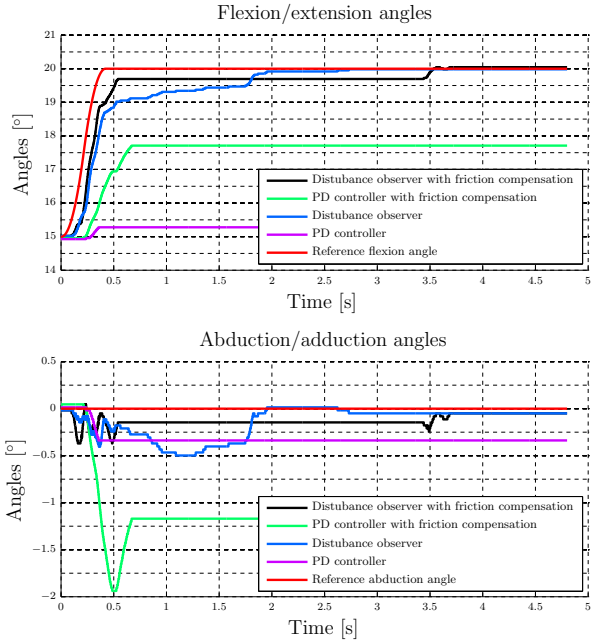

(a) Only flexion command

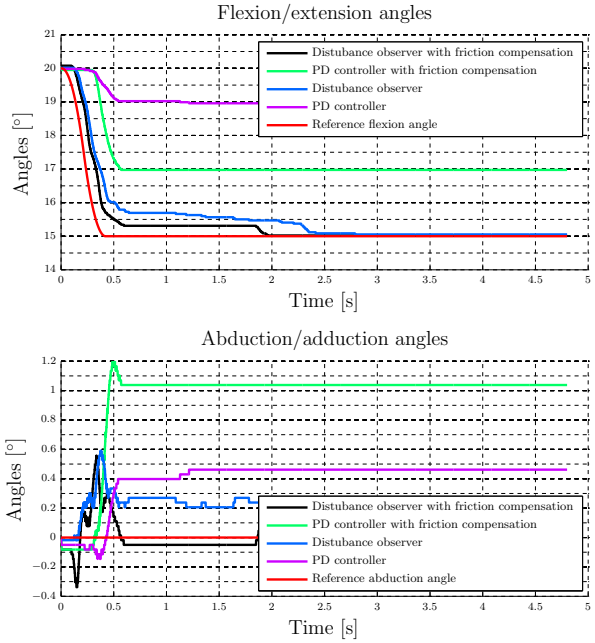

(b) Only extension command

Figure B.1

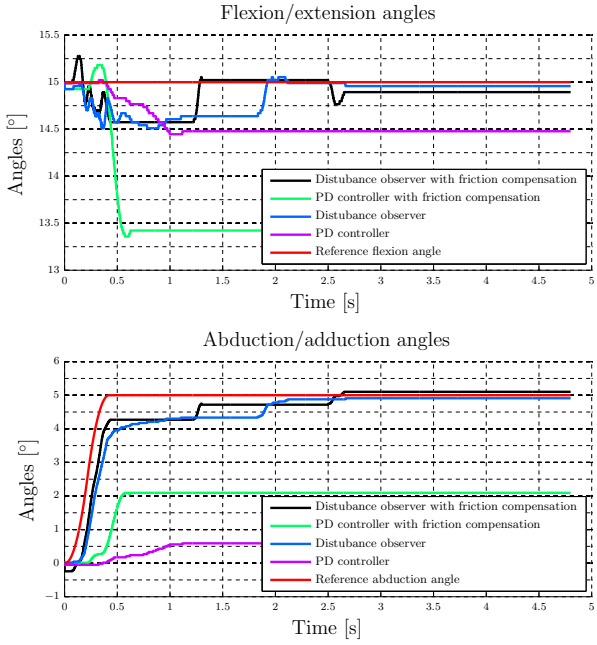

(c) Only abduction command

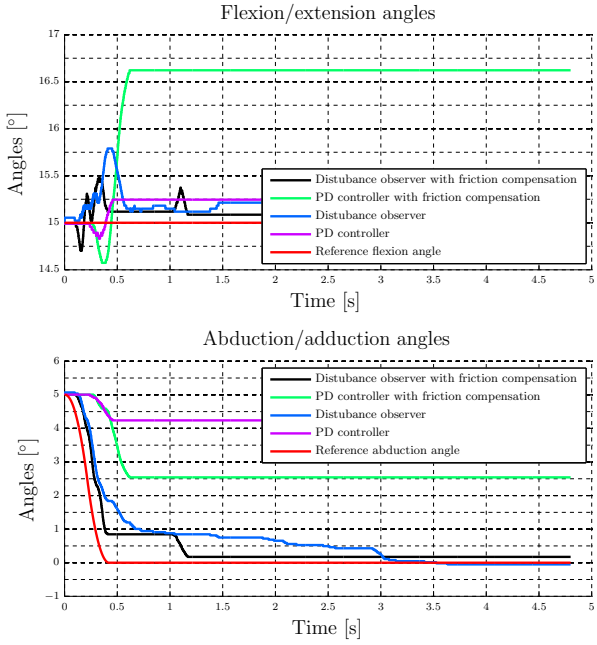

(d) Only adduction command

Figure B.1

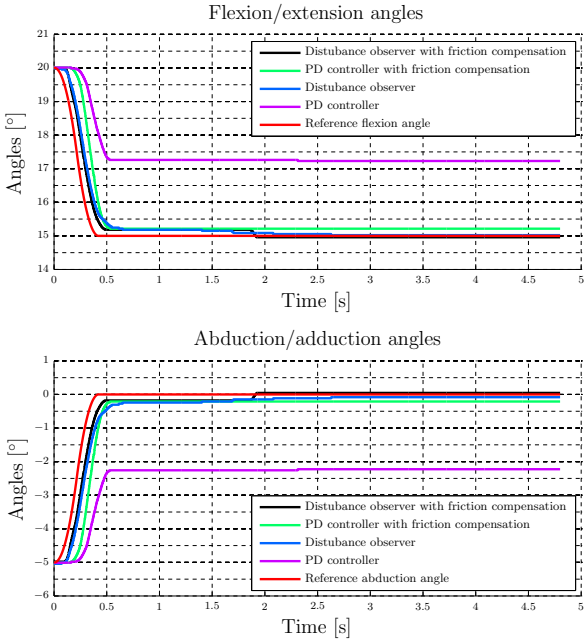

(e) Flexion and abduction along the 2^{nd} motor

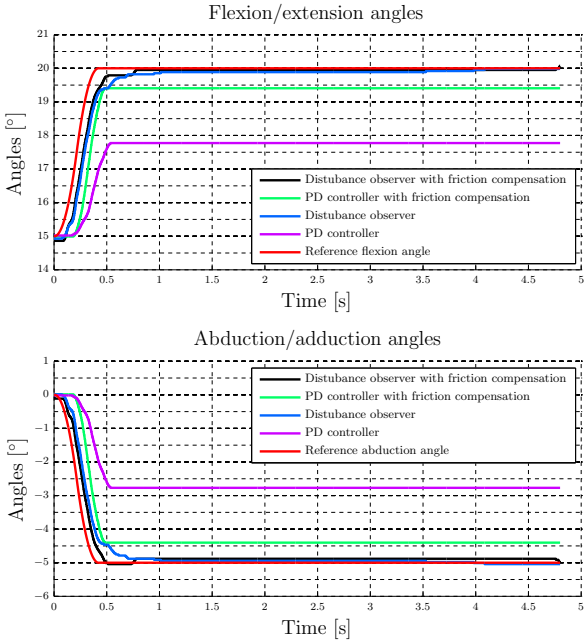

(f) Extension and adduction along the 2^{nd} motor

Figure B.1

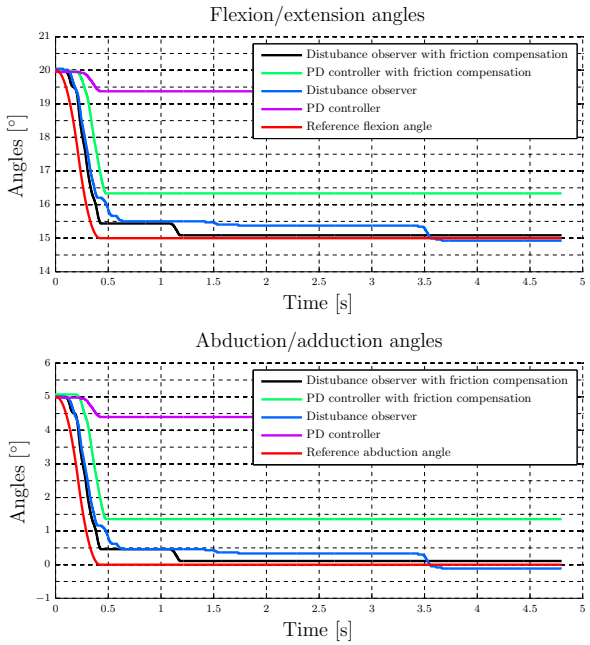

(g) Flexion and abduction along the 3^{rd} motor

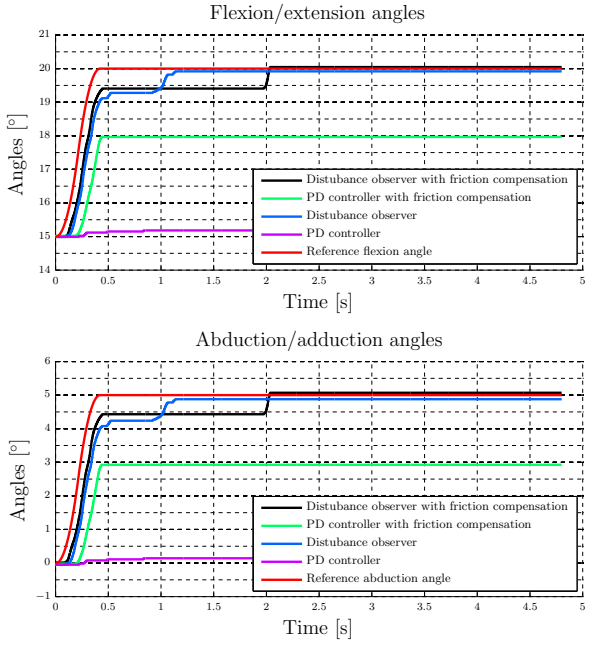

(h) Extension and adduction along the 3^{rd} motor

Figure B.1: Blended trajectory (trapezoidal velocity profile) reference - responses of the DOB based controller (with and without friction compensation) and the PD controller (with and without friction compensation)

Bibliography

A. Bicchi. Hands for dexterous manipulation and robust grasping: a difficult road toward simplicity. *IEEE Transactions on Robotics and Automation*, 16(6):652 –662, Dec. 2000. ISSN 1042-296X. doi: 10.1109/70.897777.

C. Canudas-de Wit, H. Olsson, K.J. Astrom, and P. Lischinsky. A new model for control of systems with friction. *IEEE Transactions on Automatic Control*, 40(3):419 –425, Mar. 1995. ISSN 0018-9286. URL 10.1109/9.376053.

C.P. Connette. Technical report, Deutsches Zentrum für Luft- und Raumfahrt e.V. (DLR), Oberpfaffenhofen, Apr. 2006.

P.R. Dahl. A solid friction model. Technical report, Aerospace Corp El Segundo CA, May 1968.

DLR-Website. Multisensorielle 5-Finger-Hand, Aug. 2011a. URL http://www.dlr.de/desktopdefault.aspx/tabid-3432/7418_read-12775/7418_page-6/gallery-1/51_read-9/.

DLR-Website. DLR Light-Weight Robot (LWR), Aug. 2011b. URL http://www.dlr.de/rm/desktopdefault.aspx/tabid-3803/6175_read-8963/.

R. Fletcher and C. M. Reeves. Function minimization by conjugate gradients. *The Computer Journal*, 7(2):149–154, Feb. 1964.

W. B. Griffin, R. P. Findley, M. L. Turner, and M. R. Cutkosky. Calibration and mapping of a human hand for dexterous telemanipulation. *ASME IMECE 2000 Conference Haptic Interfaces for Virtual Environments and Teleoperator Systems Symposium*, 2000.

G. Hirzinger, B. Brunner, J. Dietrich, and J. Heindl. Rotex - the first remotely controlled robot in space. In *Proceedings of the International Conference on Robotics and Automation '94*, pages 2604–2611, 1994.

H. Hu, X. Gao, J. Li, J. Wang, and H. Liu. Calibrating human hand for teleoperating the HIT/DLR Hand. In *Proceedings of the IEEE International Conference on Robotics and Automation, 2004.*, volume 5, pages 4571 – 4576, Apr. 2004. doi: 10.1109/ROBOT.2004.1302438.

M. Huenerfauth and P. Lu. Calibration guide for cyberglove. Technical report, The City University of New York (CUNY), n.d.

K. Landzettel, C. Preusche, A. Albu-Schäffer, D. Reintsema, D. Rebele, and G. Hirzinger. Robotic on-orbit servicing - DLR's experience and perspective. In *Proceedings of the IEEE/RSJ International Conference on Intelligent Robots and Systems, 2006.*, pages 4587 –4594, Oct. 2006. doi: 10.1109/IROS.2006.282164.

L. Le Tien, A. Albu-Schäffer, A. De Luca, and G. Hirzinger. Friction observer and compensation for control of robots with joint torque measurement. In *Proceedings of the IEEE/RSJ International Conference on Intelligent Robots and Systems, 2008.*, pages 3789 –3795, Sep. 2008. doi: 10.1109/IROS.2008.4651049.

H.S. Lee and M. Tomizuka. Robust motion controller design for high-accuracy positioning systems. *IEEE Transactions on Industrial Electronics*, 43(1):48 –55, Feb. 1996. ISSN 0278-0046. URL `10.1109/41.481407`.

D. Lichtblau and E.W. Weisstein. Mathworld–a wolfram web resource condition number., Aug. 2011. URL `http://mathworld.wolfram.com/ConditionNumber.html`.

H. Liu, K. Wu, P. Meusel, N. Seitz, G. Hirzinger, M.H. Jin, Y.W. Liu, S.W. Fan, T. Lan, and Z.P. Chen. Multisensory five-finger dexterous hand: The DLR/HIT Hand II. In *Proceedings of the IEEE/RSJ International Conference on Intelligent Robots and Systems, 2008.*, pages 3692–3697, Sep. 2008.

H. Olsson, K. J. Astrom, C. Canudas-de Wit, M. Gafvert, and P. Lischinsky. Friction models and friction compensation. *Eur. J. Control*, 4(3):176–195, 1998.

C. Preusche, D. Reintsema, T. Ortmaier, and G. Hirzinger. The DLR telepresence experience in space and surgery. In *Joint International Coe/Ham-SFB453 Workshop On Human Adaptive Mechatronics And High Fidelity Telepresence*, Oct. 2005.

A. Sabanovic and K. Ohnishi. *Motion Control Systems*. John Wiley & Sons(Asia) Pte Ltd, Singapore, 2011.

B. Sommer. Automation and robotics in the German space program - unmanned on-orbit servicing (OOS) and the Tecsas mission. In *Proceedings of 55th International Astronautical Congress, Vancouver ; Canada*, Oct. 2004.

E. Stoll, U. Walter, J. Artigas, C. Preusche, P. Kremer, G. Hirzinger, J Letschnik, and H. Pongrac. Ground verification of the feasibility of telepresent on-orbit servicing. *J. Field Robotics*, 26(3):287–307, 2009.

L. Tarabini, J. Gil, F. Gandia, M.A. Molina, J.M. Del Cura, and G. Ortega. Ground guided cx-olev rendez-vous with uncooperative geostationary satellite. *Acta Astronautica*, 61(1-6):312 – 325, Jun.-Aug. 2007.

T. Tsuji, K. Natori, H. Hishi, and K. Ohnishi. A controller design method of bilateral control system. In *European Power Electronics and Drives Journal*, volume 16, pages 328 –333, May 2006.

T. Tsuji, K. Ohnishi, and A. Sabanovic. A controller design method based on functionality. *IEEE Transactions on Industrial Electronics*, 54(6):3335 –3343, Dec. 2007. ISSN 0278-0046. doi: 10.1109/TIE.2007.906175.

B. Wang and S. Dai. Dataglove calibration with constructed grasping gesture database. In *Proceedings of the IEEE international conference on Virtual Environments, Human-Computer Interfaces and Measurement Systems, 2009.*, VECIMS'09, pages 6–11, Piscataway, NJ, USA, 2009. IEEE Press. URL `http://portal.acm.org/citation.cfm?id=1699798.1699800`.

Wikipedia. Anaxagoras — Wikipedia, the free encyclopedia, Aug. 2011a. URL `http://en.wikipedia.org/wiki/Anaxagoras`.

Wikipedia. Aristotle — Wikipedia, the free encyclopedia, Aug. 2011b. URL `http://en.wikipedia.org/wiki/Aristotle`.

J. Zhou, F. Malric, and S. Shirmohammadi. A new hand-measurement method to simplify calibration in cyberglove-based virtual rehabilitation. *IEEE Transactions on Instrumentation and Measurement*, 59(10):2496 – 2504, Oct. 2010. ISSN 0018-9456. doi: 10.1109/TIM.2010.2057712.

Typeset October 21, 2011